ANNALS OF GEOPHYSICS, 69, 6, 2026; doi:10.4401/ag-9605
OPEN ACCESS

Integrated Geophysical Protocols for the Characterization of Active and Capable Faults (FAC) in Volcanic Environments: The Mount Etna Case Study

Grazia Maria Caielli[*,1], Roberto de Franco[1], Sabatino Piscitelli[2], Iacopo Nicolosi[3], Vincenzo Sapia[3], Valerio Materni[3], Vincenzo Di Fiore[4], Luca Maria Puzzilli[5], Sebastiano Imposa[6], Raffaele Azzaro[3], Jessica Bellanova[2], Graziano Boniolo[1], Giulio Brunelli[3], Giuseppe Calamita[2], Stefano Catalano[6], Giuseppe Cavuoto[4], Federica Davani[1,7], Francesca D'Ajello Caracciolo[3], Gregory De Martino[2], Daniela Famiani[3], Ivan Ferrari[4], Sabrina Grassi[6], Salomon Hailemikael[3], Marco Mancini[1], Gabriele Morreale[6], Daniela Niceforo[5], Francesca Pacor[3], Edoardo Peronace[1], Angela Perrone[2], Claudia Pirrotta[6], Attilio Porchia[1], Michele Punzo[4], Gabriele Quattrocchi[6], Valerio Ruscito[5], Maurizio Simionato[1], Daniela Tarallo[4], Antonio Torrisi[8], Giuseppe Tortorici[1], Iolanda Gaudiosi[1]

(1) Istituto di Geoscienze, Consiglio Nazionale delle Ricerche, Italy
(2) Istituto di Metodologie Integrate per l'Osservazione della Terra, Consiglio Nazionale delle Ricerche, Italy
(3) Istituto Nazionale di Geofisica e Vulcanologia, Italy
(4) Istituto di Scienze del Patrimonio Culturale, Consiglio Nazionale delle Ricerche, Italy
(5) Istituto Superiore per la Protezione e la Ricerca Ambientale, Rome, Italy
(6) Università di Catania, Dipartimento di Scienze Biologiche, Geologiche e Ambientali (DSBGA), Catania, Italy
(7) Università di Trieste, Dipartimento di Matematica, informatica e Geoscienze, Trieste, Italy
(8) Dipartimento Regionale Protezione Civile della Presidenza della Regione Siciliana, Nicolosi (CT), Italy

Article history: received April 30, 2026; accepted November 12, 2026

Abstract

This study presents the development and application of integrated geophysical protocols designed for the identification and characterization of Active and Capable Faults (Faglie Attive e Capaci; FAC) within the volcanic context of Mount Etna, as part of the Etna FAC_MS Project. The need for site-specific guidelines (LG_FAC_Etna) arises from the distinctive structural and kinematic features of the Etnean region, where tectonic faulting interacts with magmatic processes and gravitational flank instability.

Through a multi-methodological approach conducted across representative sites, including the Fiandaca, Pernicana, and Timpe fault systems, techniques such as Electrical Resistivity Tomography (ERT), Ground Penetrating Radar (GPR), seismic refraction/reflection (SR), and Horizontal-to-Vertical Spectral Ratio (HVSR) measurements were employed. The research defines four conceptual geophysical models (exposed faults, buried faults, active fracture zones, and aseismic creep zones) to translate geological evidence into measurable physical signals, such as resistivity gradients and seismic wave velocity variations.

The results demonstrate that the integration of high-resolution surveys significantly reduces uncertainty in the inferred location and spatial extent of fault-related deformation zones. This facilitates the transition from Level 1 "Areas of Attention" (ZA) to Level 3 "Respect Zones" (ZR)

and “Susceptibility Zones” (ZS), providing a fundamental framework for land-use planning and seismic risk mitigation in densely urbanized volcanic areas.

Keywords: Active and Capable Faults (FAC); Mount Etna Context; Geophysical surveys; Geophysical protocols of measurements

1. Introduction

Within the framework of the Etna FAC_MS Project, a collaboration between the Regional Department of Civil Protection of Sicily (DRPC Sicilia) and the Italian National Research Council – Institute of Environmental Geology and Geoengineering (CNR-IGAG), representing the Center for Seismic Microzonation (CentroMS), specific guidelines (LG_FAC_Etna) have been developed for identifying and characterizing Active and Capable Faults (FAC) in the Etnean volcanic area (Gruppo di lavoro ETNA FAC, 2024).

The primary objective of this task is to provide standardized and shared tools for identifying and assessing the fault systems that characterize the Etna region. These guidelines complement the 2015 national standards (Linee Guida FAC, 2015) issued by the Technical Commission for Seismic Microzonation (MS). They offer specialized technical support and interpretative tools for land-use planning and risk mitigation, incorporating extensive geological, geodetic, and seismic datasets collected over recent decades.

The necessity for these specific guidelines derives from the unique structural and kinematic features of the region’s active tectonics, which often diverge from the standard definitions and predictive mapping criteria established for Apennine and Alpine settings. The structural architecture of Mt. Etna is governed by the interplay between regional lithospheric structures, primarily the Hyblean-Malta Escarpment and the Messina-Etna fault system, and local stress fields induced by magma dynamics.

This complex tectono-volcanic setting exposes the region to two main sources of seismic hazard:

- Regional Tectonic Earthquakes: High-magnitude events (e.g., 1169, 1693, 1908; M ≈7.3) that have historically devastated eastern Sicily.
- Volcano-Tectonic Events: More frequent, lower-magnitude events (M ≤ 5.0). Despite their lower energy, these cause disproportionate damage due to extremely shallow focal depths (2-4 km) and concentrated effects along fault traces, often occurring in swarms during volcanic eruptions (e.g., the December 2018 Mw 4.9 Fiandaca earthquake).

Detecting FAC in volcanic environments is one of the most significant hurdles in modern geophysics. The complex subsurface, characterized by irregular successions of ash and lava, scatters seismic signals and obscures fault geometries. To this complexity is added a high background noise from constant volcanic tremors and anthropogenic interference in densely urbanized areas. Furthermore, isolating tectonic fault activity is challenging as it is often inextricably linked with magma inflation, hydrothermal fluid migration, and the gravitational spreading of the volcanic edifice.

In this context, geophysical and geognostic investigations (Level 3 MS) are essential for the integration and validation of primary data. These investigations refine the information acquired through Level 1 MS (aerial photogrammetric analysis) and Level 2 MS (geological/geomorphological mapping) surveys, providing a physical basis for defining “Respect” and “Susceptibility” zones.

The active features of Mt. Etna cataloged as capable faults (ITHACA Working Group, 2019), have been classified for MS purposes based on their surface expression and kinematic behavior:

- FAC (Active and Capable Faults): Structures with a documented seismic history and associated ground rupture, categorized as $FAC_{_a}$ (certain trace) or $FAC_{_b}$ (uncertain/buried trace).
- ZFA (Active Fracturing Zones): These represent areas potentially subject to coseismic ground rupture where a single fault trace cannot be isolated (e.g., secondary conjugate systems). These envelopes often extend beyond the canonical widths defined by national guidelines and require specific land-use planning constraints.
- Aseismic Creep Faults: Included due to their significant territorial impact and frequent physical continuity with seismogenic segments.

This paper presents the results of the Level 3 MS geophysical planning conducted on representative sample sections of the FAC. By employing a multi-methodological approach, including high-resolution electrical and seismic surveys, we evaluate the professional standards required to characterize fault-related deformation in urban and suburban volcanic settings. The study demonstrates how the integration of these advanced geophysical investigations into the LG_FAC_Etna framework provides a more robust and replicable methodology for risk mitigation in high-risk volcanic regions.

2. Geological and Tectonic Setting of Mount Etna

2.1 Regional Tectonic Framework

Mount Etna is located in a complex tectonic setting in the central Mediterranean, where the ongoing convergence between the African and Eurasian plates interacts with major lithospheric structures. The volcano sits upon the footwall of the Malta Escarpment, a major NNW-SSE trending crustal discontinuity separating the African continental shelf from the Ionian oceanic basin. This regional setting exerts primary control on Etnean activity: the E-W extensional regime associated with the rollback of the Ionian subducting slab facilitates magma ascent, while the regional compressive stress field influences the orientation of the feeder systems and the structural architecture of the Sicilian orogen.

2.2 Local Structural Framework and Fault Characterization

In the Etnean context, an Active and Capable Fault (FAC) is defined by its ability to produce significant surface deformation within the current tectonic regime. Unlike purely tectonic regions, Etna's faults exhibit a wide spectrum of deformational behaviors:

- Seismic Slip: High-frequency energy release (e.g., the 2018 Mw 4.9 Fiandaca event).
- Aseismic Creep: Continuous or episodic slow-motion displacement (e.g., 20-30 mm/a on the Pernicana Fault).
- Earthquake Swarms: Clusters of low-to-moderate magnitude events often associated with magmatic dikes.
- Surface Coseismic Faulting: Ground ruptures occurring even on "hidden" segments of seismogenic structures lacking permanent morphological scarps.

The edifice is affected by several volcano-tectonic structures predominantly distributed across the eastern sector (Azzaro et al., 2012). Two extensive eruptive rifts bound this area: the South Rift (N-S to NNE-SSW) and the North-East Rift (NE-SW).

2.3 Detailed Description of Active Fault Systems

The major fault systems are categorized by their location and kinematics, primarily following the "Volcano-tectonic map of Mount Etna" (Azzaro et al., 2012):

2.3.1 The Pernicana and Southern Shear Zones

The Pernicana Fault is a major left-lateral transform structure extending for ≈20 km with a dip to the south. Its eastern sector is dominated by aseismic creep (20-30 mm/a), while the western portion is seismogenic with a prominent normal component and a distinct scarp. To the south, the rift transitions into a right-oblique shear zone featuring the Tremestieri and Trecastagni faults (NW-SE trending; NE dipping; Branca et al., 2015).

The Tremestieri Fault (≈7 km) offsets Holocene flows with an estimated slip rate of 4 mm/a. Its northern reaches are "hidden," with seismic epicenters clustering near Mascalucia and Nicolosi.

The Trecastagni Fault (≈7 km) shows seismic activity only in its northern portion, where a scarp is well-developed. The structure undergoes aseismic creep monitored by extensometers (Gambino et al., 2011; Bonforte et al., 2013), with a slip rate of ≈4 mm/a.

2.3.2 The Timpe System and Hidden Seismogenic Structures

The eastern flank is dominated by the Timpe system (Fig. 1), a bundle of NNW-SSE-striking, E-dipping normal faults including (Azzaro et al., 2012, 2013):

- Acireale Fault: Displays a 120 m high scarp and a vertical slip rate of 1.3-4.3 mm/a.
- Moscarello Fault: Features scarps up to 150 m high with vertical slip rates between 1.4 and 2.7 mm/a.
- San Leonardello and Macchia Faults: Cut through the Holocene "Chiancone" formation with scarps of 20 m and 10 m respectively, (Azzaro et al., 2020). Vertical slip rates (<8 ka) are 2.6 mm/a (S. Leonardello) and 1.3 mm/a (Macchia).

Further, inland, the Fiandaca, Santa Tecla, and Santa Venerina faults are significant seismogenic structures. While often "hidden," they produce extensive zones of coseismic faulting. During the 2018 Mw 4.9 earthquake, the fractured zone along the Fiandaca Fault reached widths of several hundred meters (Civico et al., 2019; Tortorici et al., 2021; Azzaro et al., 2022), highlighting the high uncertainty in the spatial distribution of fracturing of hidden segments. The Santa Tecla Fault shows a vertical slip rate of ≈4.3 mm/a (over 35 ka), while the Santa Venerina Fault was identified following the 2002 earthquake.

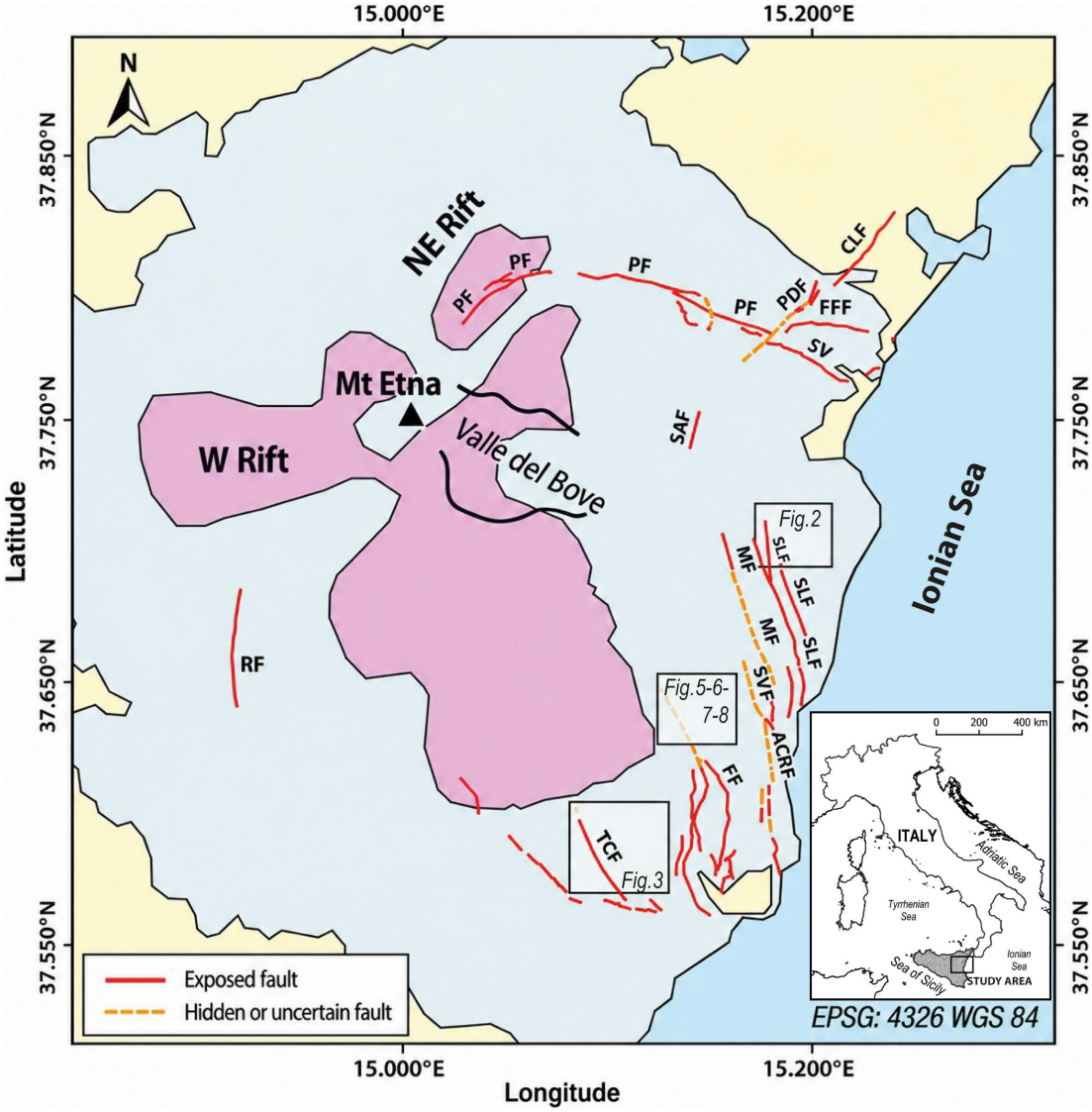

Figure 1. Schematic diagram and morphological expression of the main active volcano-tectonic structures. Fault abbreviations: **PF**, Pernicana; **RF**, Ragalna; **TCF**, Trecastagni; **FF**, Fiandaca; **ACRF**, Acireale; **MF**, Moscarello; **SLF**, S. Leonardello; **SVF**, S. Venerina; **PDF**, Piedimonte; **FFF**, Fiume Freddo; **CLF**, Calatabiano; **SV**, S. Venera; **SAF**, S. Alfio. Modified and updated after Azzaro et al., 2012.

2.4 Flank Instability and Tectonic-Magmatic Coupling

The eastern and south-eastern flanks undergo continuous seaward instability toward the Ionian Basin. This process results from a synergy between three drivers:

- Regional Tectonics: Plate convergence and E-W extension providing the structural framework for lateral displacement.
- Basement Geometry: A weak, clay-rich sedimentary basement acting as a décollement surface.
- Magmatic Intrusions: High-pressure dike injections along the rifts acting as a "hydraulic jack," generating lateral overpressure that accelerates flank motion.

This instability activates the bounding faults: the Pernicana system acts as a northern decoupling boundary, while the Timpe system accommodates extension at the toe of the slope. This creates a feedback loop where flank movement opens pathways for magma.

2.5 Geological Setting and Mapping Discrepancies

Stratigraphically, the Etnean district evolved from marine volcanism (~500 ka) to subaerial activity (~330 ka) (De Beni et al., 2011). Mapping these units (e.g., CARG project 1:50,000 scale, specifically for Sheet 625 Acireale; Servizio Geologico d'Italia, 2009) relies on lithostratigraphic and synthemic categories. However, a significant discrepancy exists between standard geological maps and volcano-tectonic needs:

- CARG Project Map (1:50,000): Includes only segments with clear geological/morphological evidence of displacement.
- Volcano-tectonic Map (Azzaro et al., 2012): Documents hidden seismogenic segments capable of surface faulting, based also on historical data (Azzaro, 1999) and recent events (Romagnoli et al., 2021).

The study areas selected are based on the FAC and associated Attention Zones (ZA), utilizing 1:10,000 scale high-resolution field surveys to refine the existing 1:50,000 geological database (Branca et al., 2011).

3. Geophysical Protocols for Active and Capable Fault (FAC) Detection: Integrated Approaches and Case Studies

3.1 Framework and Objectives

In accordance with the national guidelines for Seismic Microzonation (Linee Guida FAC, 2015), geophysical and geognostic investigations are fundamental for the identification and characterization of Active and Capable Faults (FAC). The primary objective is to refine the spatial and structural definition of these features, facilitating the transition from Level 1 (MS1) FAC "Attention Zones" (ZA) to Level 3 (MS3) "Susceptibility" (ZS) and "Respect Zones" (ZR).

Within this methodological framework, the study aims to:

- Map buried structures and define the geometry of the fault-affected volumes.
- Characterize subsoil geophysical parameters to evaluate potential co-seismic effects.
- Quantify uncertainties and delineate the precise spatial extent of FAC zones to support urban planning and risk-reduction strategies.

To achieve these objectives, the protocol incorporates a series of coordinated technical tasks designed to integrate new measurements with existing datasets, ensuring a robust multi-parametric approach:

- Data Integration and Traceability: Systematic analysis of geophysical surveys and population of the project database to ensure data traceability and accessibility.
- Critical Review and Reinterpretation: Evaluation of MS1 data (e.g., HVSR, SR, and ERT) to provide a high resolution characterization of FAC related anomalies.
- Methodological Standardization: Development of formal acquisition and processing protocols to maintain methodological consistency across diverse geological settings.

– Quantitative Zonation: Application of updated classification systems to various fault typologies to validate the transition from ZA to ZS/ZR zones.
– Field Investigations: Planning and execution of supplementary field investigations to resolve local uncertainties and refine the subsoil model where existing data are insufficient.

3.2 Classification of Etnean FAC and conceptual geophysical models

Geophysical conceptual models represent the "geophysical signature" of the geological-structural, lithological, and geomorphological characteristics of a FAC. Therefore, geophysical models should not be considered as a 'translation' of the corresponding geological models, but rather as their 'geophysical representation,' which intrinsically depends on the parameterization, resolution, precision, and accuracy of the models themselves. Furthermore, in a complex geological reality such as a volcano-tectonic environment, the coexistence of different types of FAC in the same area cannot be excluded; this represents an additional factor of complexity establishing the correspondence between geological and geophysical models.

The geophysical investigations can confirm and integrate results and information derived from other surveys such as aerophotogrammetric surveys, geological mapping, and morphological analysis (ind_1 and ind_2 in Linee Guida FAC, 2015).

In volcano-tectonic environments like Mt. Etna, a FAC can be identified through three main geophysical signatures:
– Genuine or primary discontinuity: A plane or surface placing different or displaced units in lateral contact.
– Non-Genuine or secondary discontinuities: A transition zone characterized by a high lateral gradient.
– Deformation Fields: Zone of variations in geophysical attributes related to fracture fields or transfer zones.

The term 'genuine or primary discontinuity' is used here in a geological sense and does not imply that a discrete fault plane is directly imaged by all geophysical methods. In ERT and travel time tomography, fault-related structures are generally inferred from lateral gradients or anomalous zones within smooth inverted resistivity or velocity fields. Their apparent width may exceed the actual width of the structural discontinuity because of finite spatial resolution, acquisition geometry, and inversion regularization. In seismic reflection and GPR data, faulting is generally inferred from offsets, terminations, or spatially coherent changes in reflectors rather than from direct reflections from the fault plane. Accordingly, the interpretations presented below refer to fault-related geophysical signatures and inferred deformation zones.

The effectiveness of these methods depends on the contrast in geomechanical attributes induced by the fault.

It must be emphasized that the effectiveness of geophysical investigations in highlighting the FAC presence highly dependents on the lateral and vertical heterogeneity induced by the faulting process on the geophysical and geomechanical attributes of the subsurface. The variations in these attributes must be significant enough to be detectable through the reconstruction of the geophysical model. For example, a strike-slip fault that does not produce a surrounding fracture or alteration zone characterized by significant dimensions and variations in geophysical parameters (at the metric to decametric scale) will almost certainly not be detectable by the standard geophysical investigations proposed here.

Table 1 summarizes the four operational geophysical conceptual models adopted for the Etnean volcanic setting (Azzaro et al., 2012). These categories are not intended to replace or modify the FAC classification of the national guidelines (Linee Guida FAC, 2015), but to distinguish recurring structural/deformation settings that require different geophysical investigation and interpretation strategies. Within this framework, 'geophysical attributes' refer to two main categories: (i) physical parameters, such as resistivity and P/S-wave velocities, derived from 2D and pseudo-2D parametric inversion (e.g., ERT, Seismic Tomography, SR, Multichannel Analysis of Surface Waves; MASW, and HVSR); and (ii) signal characteristics, such as amplitude and phase, which define the reflected field and seismic facies through 2D seismic and GPR imaging.

Table 1. Main geophysical evidence and geological/geomorphological consistency criteria for the Etna-specific operational geophysical conceptual models.

Geophysical conceptual model	Main geophysical evidence	Geological/geomorphological features
FAC_E *Exposed Fault*	High lateral gradients in resistivity and/or seismic velocity fields; displacement or steps in refracting interfaces; lateral variation in HVSR attributes; displaced or interrupted reflectors in seismic and/or GPR sections.	Consistency with a mapped surface fault trace, fault scarp, morphological discontinuity, and/or documented coseismic surface rupture.
FAC_{E_S} *Buried Fault*	Lateral gradients or displacements of layers beneath a surface cover; variations in geophysical attributes that can be followed laterally under cover deposits; displaced or interrupted reflectors at depth.	Possible correspondence with surface flexure or other indirect morphological evidence; the main structural discontinuity is not directly exposed at the surface.
ZFA *Active Fracturing*	Lateral variations of the geophysical attribute not attributable to a single lineament, locally lower seismic velocities, resistivity anomalies depending on saturation and alteration, complex reflectivity and signal scattering.	Correspondence with broad zones of coseismic surface fracturing, secondary structures, fracture fields, and/or transfer zones. The limits of the deformation zone may not correspond with a single morphological discontinuity.
FAC_{E_C} *Aseismic Creep*	Metric to decametric zone characterized by lateral variation of geophysical attributes while maintaining partial layer continuity; possible evidence of shallow deformation or slip surfaces where supported by the data.	Consistency with documented aseismic creep, progressive surface deformation, morphological variations, surface fracturing, and/or sectors where aseismic and coseismic deformation coexist.

3.3 Criteria for identifying geophysical investigation areas

The definition of the geophysical investigation areas and the identification of FAC attention zones were obtained by analyzing available previous literature data along with the Etna fault catalogues (Azzaro et al., 2012 and ITHACA catalog).

In the Etna area, and generally in volcano-tectonic environments structural complexity is reflected in the heterogeneity of physical parameters over spatial scales ranging from meters to decameters and in strong contrasts in geophysical and geotechnical properties.

The identification of FAC areas and their respective attention zones was proposed in the MS1 studies previously conducted in the Etna area by professionals. The MS1 studies involved both the collection and cataloguing of all previous geophysical surveys with geological field surveys and data useful for the study, as well as the execution of new investigations, both linear and punctual. The integration of geophysical surveys in Level MS1 was primarily aimed at identifying areas susceptible to local site effects and providing indicative information on the FAC and their related ZA and did not follow a planning process based on the specific definition, classification, and characterization of the Etna area FAC as outlined in this project.

3.3.1 Selection criteria and sizing of geophysical investigations (Multi-technique – Multi-scale) and operational guidelines for investigation planning

The identification of the investigation area and the planning of FAC geophysical surveys must be based on the results and information derived from ind_1 and ind_2 investigations (Linee Guida FAC, 2015), as well as on informative data regarding coseismic and post-seismic effects. It is therefore always advisable to design the geophysical survey

based on an a priori hypothesis of the FAC's existence (including its characteristics according to classification) and/or the zone where it may be located, or where associated structural elements such as further conjugate planes and/or fracturing zones can be hypothesized.

To overcome the intrinsic non-uniqueness of geophysical models, an integrated multi-methodological approach is required. In complex volcanic settings, 2D techniques are preferred over 1D models to capture lateral heterogeneities. When performing surveys with different techniques in the same area, it is advisable to conduct them, whenever possible, along the same acquisition lines (transects) used for each specific technique. The recommended 2D geophysical techniques are ERT, GPR, SR while the pseudo-2D techniques include HVSR Arrays and MASW acquired in a roll-along configuration.

The sizing of the surveys and the sampling of areas with hypothesized FAC must be carried out, provided they are logistically feasible, as follows:

a) **Perpendicular to the strike of the hypothesized FAC**:
   - The maximum survey length "should" extend laterally for at least ±150 m relative to the identified or assumed FAC trace (consistent with the maximum size of the ZS – Susceptibility Zone), plus external acquisition buffers as required by specific survey techniques.
   - The survey length must be longer than ±15 m (consistent with the maximum size of the ZR – Respect Zone), in addition to any specific acquisition buffer.

b) **Parallel to the strike of the fault**:
   - Surveys shall be performed with a spacing dependent on the significance level and variability of the FAC, hypothesized.

Regardless of survey orientation, isolated "spot" investigations that are not supported by geological, morphological, or geophysical evidence should be avoided. Such investigations do not allow the spatial continuity of fault and related anomalies to be assessed and may lead to an incorrect definition of ZS and ZR boundaries, particularly in buried-fault and distributed-fracturing settings.

Survey design should consider three factors. First, transect length should be sufficient to encompass the expected fault-affected zone and adjacent undisturbed sectors, based on available geological, geomorphological, and geophysical constraints. Second, sensor spacing should be selected according to the scale of the target heterogeneity; however, nominal sensor spacing should not be regarded as equivalent to the effective spatial resolution, which also depends on acquisition geometry, data quality, depth, and inversion strategy. Third, the acquisition geometry must be designed to reach the required investigation depth. Method-specific guidance for ERT, active-source seismic methods, HVSR, and GPR is provided in Appendix A.

Table 2 summarizes the main survey-design parameters adopted to achieve adequate characterization of the fault zone and its associated structural elements. The reported values are first-order planning recommendations for techniques based on discrete acquisition points or sensors. Method specific acquisition geometry and sampling requirements are provided in Appendix A. GPR spatial sampling, in particular, is frequency and wavelength dependent and is treated separately.

Table 2. First-order planning recommendations for 2D geophysical transects across suspected FACs. Recommended sensor/acquisition spacing should not be interpreted as the effective spatial resolution of the final model, which also depends on acquisition geometry, data quality, investigation depth, and inversion strategy.

Survey scale	Indicative profile length	Recommended sensor/acquisition spacing	Indicative target depth	Primary Objective
Large scale	>80 m	2.5-5.0 m	30-60 m	Mapping deep structural continuity and the lateral extent of the fault-affected zone; support definition of ZS boundaries.
Small scale	<80 m	0.5-2.5 m	5-15 m	High-density characterization of shallow fault-related deformation and improved constraint of ZR boundaries.

3.3.2 Integrated Geophysical Methodologies for FAC Characterization

The FAC characterization in complex volcano-tectonic settings, such as Mount Etna, requires an integrated multi-parametric approach 2D or pseudo 2D to resolve subsurface structural complexity and uncertainties. The methodological suite focuses on the transition from "Attention Zones" (ZA) to high-resolution "Respect" (ZR) and "Susceptibility Zones" (ZS) as defined in Linee Guida FAC 2015.

Among methodologies employed in seismic microzonation studies the Horizontal to Vertical Spectral Ratio (HVSR) method is widely utilized. Based on the work of Nogoshi and Igarashi (1970) and Nakamura (1989), this technique utilizes single station ambient vibration recordings. In particular, for FAC identification, the technique should be applied using a pseudo 2D approach identifying the resonance frequency and higher frequencies.

Seismic Refraction and Multichannel Analysis of Surface Waves (MASW) are complementary non-invasive geophysical techniques used to characterize the shallow subsurface. While refraction provides 2D profiles of Vp or Vs to map stratigraphic interfaces, MASW is integrated to retrieve Vs profiles by exploiting the dispersive nature of Rayleigh waves (Park et al., 1999; 2007), effectively reducing geological model uncertainty.

Electrical Resistivity Tomography (ERT) reconstructs a smooth distribution of subsurface electrical resistivity. Fault-related structures may therefore be inferred where significant lateral resistivity gradients or anomalous zones are consistent with independent geological or geomorphological evidence. The location and width of such anomalies should not be interpreted as a direct image of a discrete fault plane. Modern multi-electrode systems combined with advanced inversion algorithms (Loke and Barker, 1996a, 1996b; Loke et al., 2013; Binley and Slater, 2020), enable detailed 2D and 3D characterization of subsurface resistivity variations, thereby supporting the definition of geological models.

Ground Penetrating Radar (GPR) provides very high resolution for near-surface imaging; however, its effective penetration depth is strongly site-dependent. In heterogeneous volcanic successions, scattering and electromagnetic attenuation may restrict useful penetration to only a few meters, particularly at higher antenna frequencies. Therefore, antenna frequency must be selected according to the expected target depth and the local electromagnetic properties of the volcanic deposits.

In the following, we present some examples of geophysical survey results. Specifically, Fig. 2 illustrates an ERT profile conducted transversely to the San Leonardello fault (Agrumeto area), which is classified as an exposed FAC (FAC_E). A marked lateral resistivity gradient can be traced from the surface to the maximum investigated depth and is interpreted, together with the geological and morphological evidence, as a fault-related anomaly. Figure 3 shows a GPR profile performed across a FAC located in the S. Giovanni la Punta area to characterize TCF fault, where ind_1 and ind_2 investigations suggest the presence of a fault or creep zone (FAC_{E-C}). The data show deformed layers with lateral attribute variations and potential sliding surfaces, correlating with surface fracturing and documented coseismic deformation.

For further details and additional examples of geophysical investigations, refer to the FAC technical sheets described in Section 4.

4. Case studies for different FAC and geological environment

Given the high density of Active and Capable Faults (FACs) in the Etnean area, as well as the length and dimensions of the Attention Zones (ZAs) identified during the MS1 (Level 1 Microzonation) phase, the planning for MS3 geophysical surveys was conducted by selecting representative sample sections of FACs based on the following criteria:

- Geological Behavior: Selection was based on similar kinematics and deformational behavior, according to the revision and reclassification proposed in the frame of the project;
- Logistical Feasibility: Consideration of the constraints inherent to operating within densely populated urban and suburban environments.

Furthermore, the planning phase focused on employing methodologies, instruments, and measurement configurations that represent a "professional standard" within the current state-of-the-art of geophysical exploration. This ensures that the procedures remain executable by qualified professionals in accordance with these guidelines. In addition to these "standard" acquisitions, more in-depth investigations were performed on specific sections for methodological testing and research purposes.

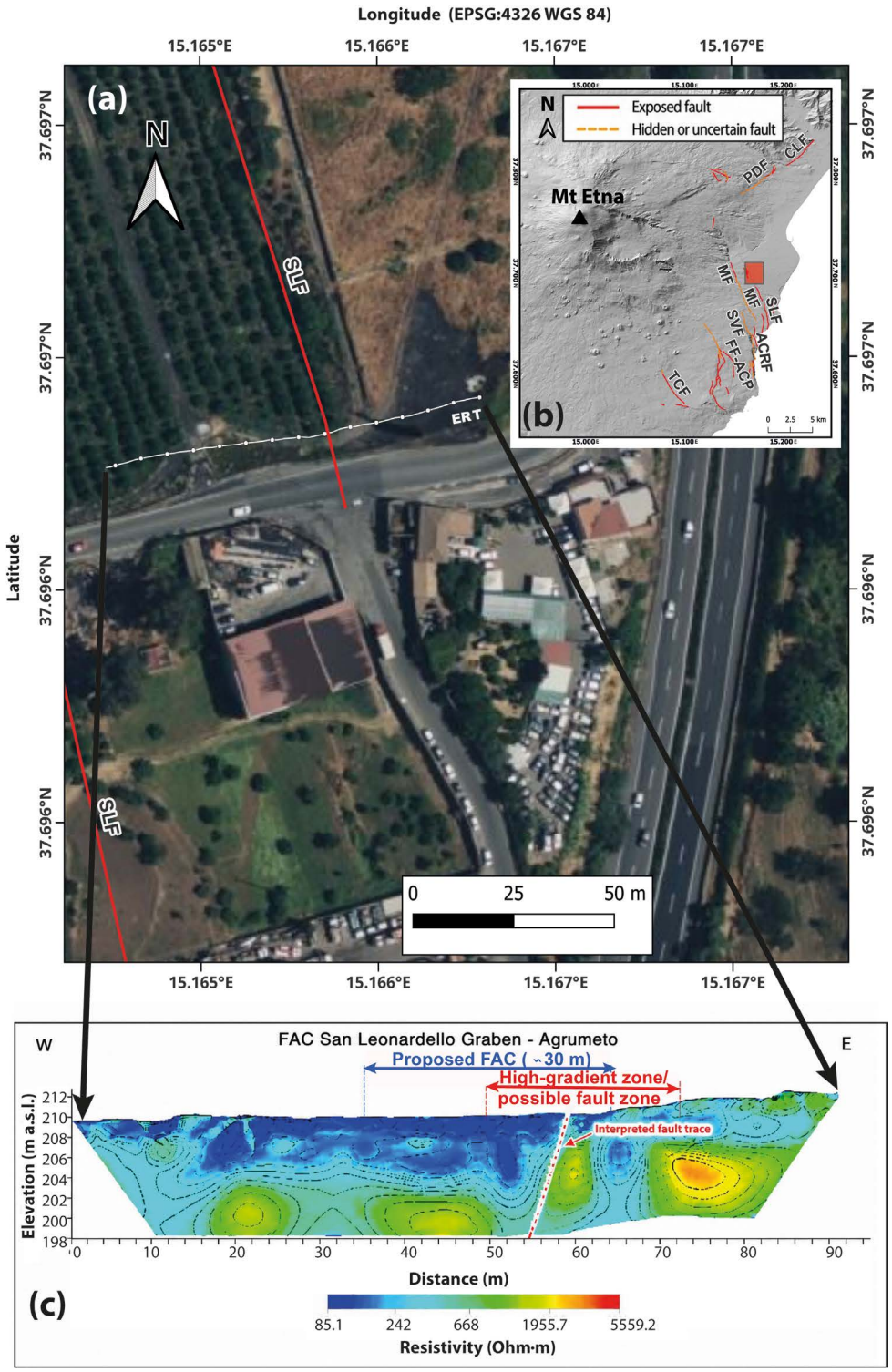

Figure 2. Geophysical characterization of the San Leonardello Fault (SLF) area (Agrumeto site). (a) Aerial view of the investigated area showing the mapped surface fault traces (SLF) and the location of the electrical resistivity tomography (ERT) profile. (b) Regional structural setting of the study area, with the main mapped fault systems; the red box indicates the location of the investigated site. (c) Electrical resistivity tomography section along the W-E profile, showing the subsurface resistivity distribution. Resistivity values are expressed in Ω·m; elevation is in metres above sea level. 2D electrical tomography section is 1 m step. Between 50-72 m, a zone of high lateral gradient resistivity is highlighted, interpretable as fault-related resistivity anomaly. The zone affected by the possible FAC extends to approximately 46 m. There is a clear correlation with the morphology, with a bed characterized by higher resistivity values. In this case, an asymmetric zone of respect (blue line) of approximately 30 m is proposed for the FAC (red dashed line).

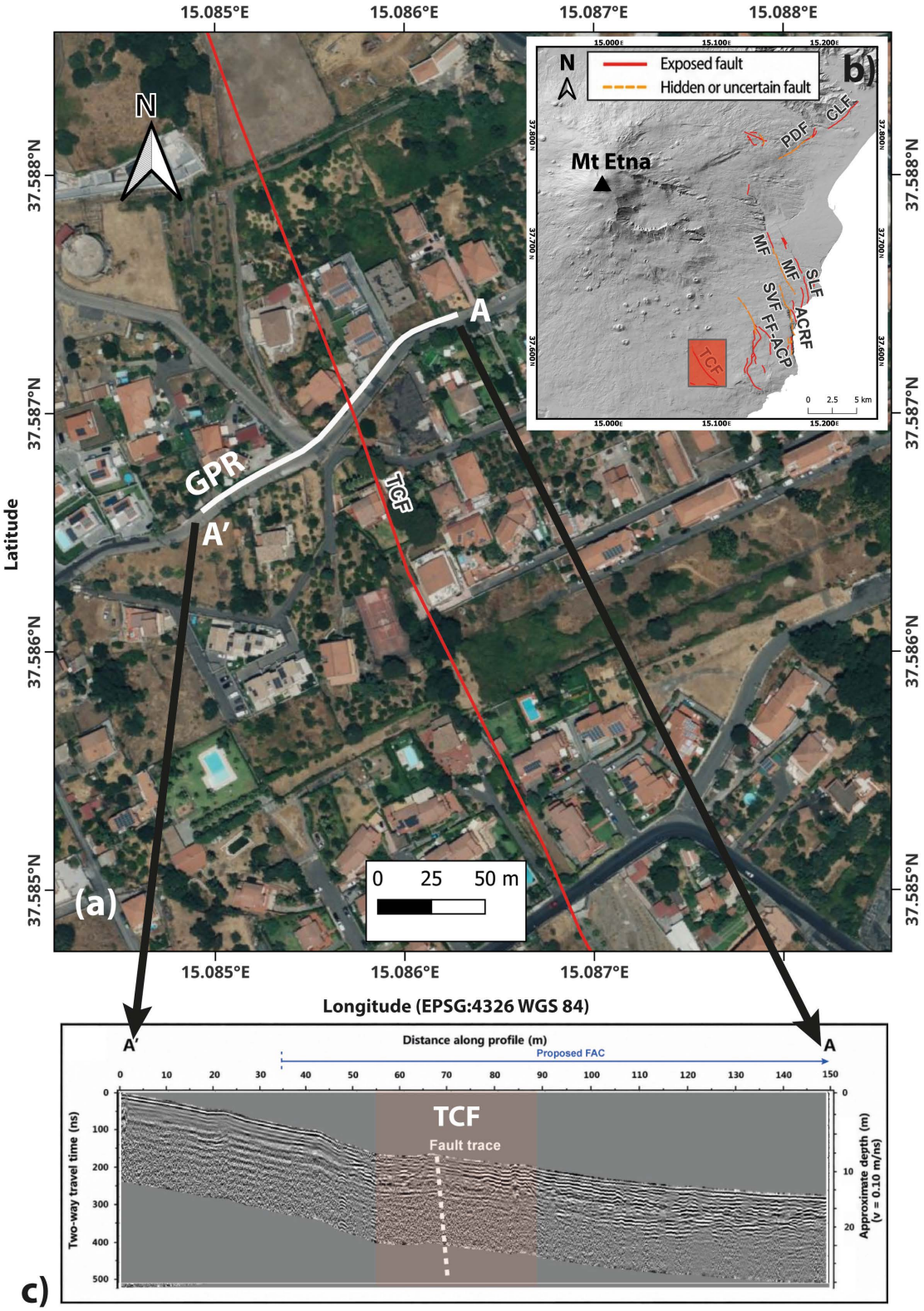

Figure 3. Geophysical characterization of the Trecastagni Fault (TCF) in San Giovanni la Punta area. (a) Aerial view of the investigated area showing the mapped fault trace (TCF) and the location of the GPR profile. (b) Regional structural framework of the study area, with the main mapped fault systems; the red box indicates the location of the investigated site. (c) GPR section. Between 50-60 m, a variation in the GPR facies is highlighted in the first 5 meters of depth. Between 40-80 m, this layer shows clear deformation correlated with a well-defined morphological variation. The surface layer (approximately 5 m deep) is confined at the bottom by a horizon that could be interpreted as a slip zone. In this case, an asymmetric susceptibility zone (blue line) of approximately 220 m in size is proposed for the FAC.

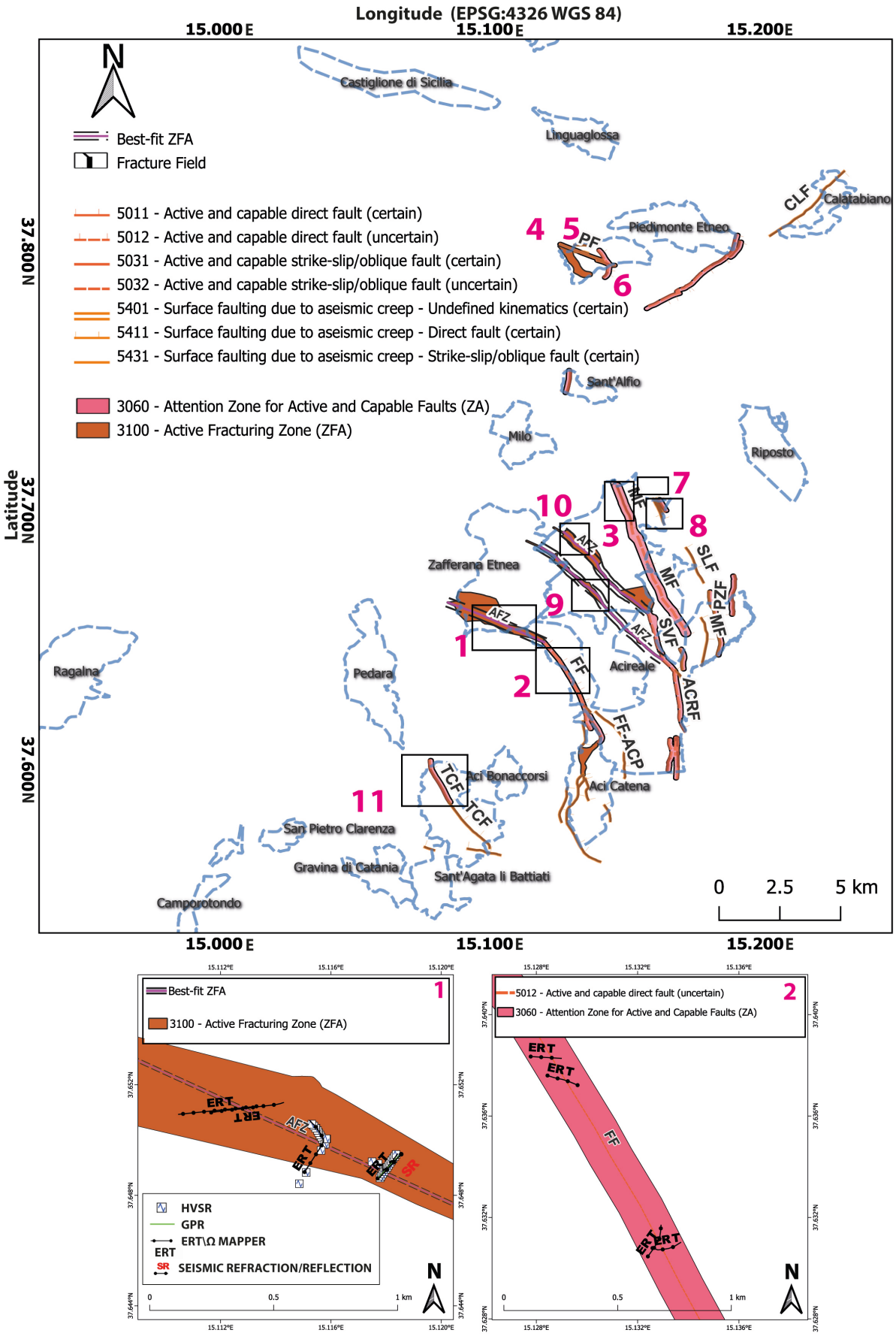

Figure 4. Example Map of the FAC segments where geophysical surveys were conducted and details of the boxes 1 and 2 showing the location of the geophysical surveys. The numbers in the boxes correspond to the IDs listed in Table 3.

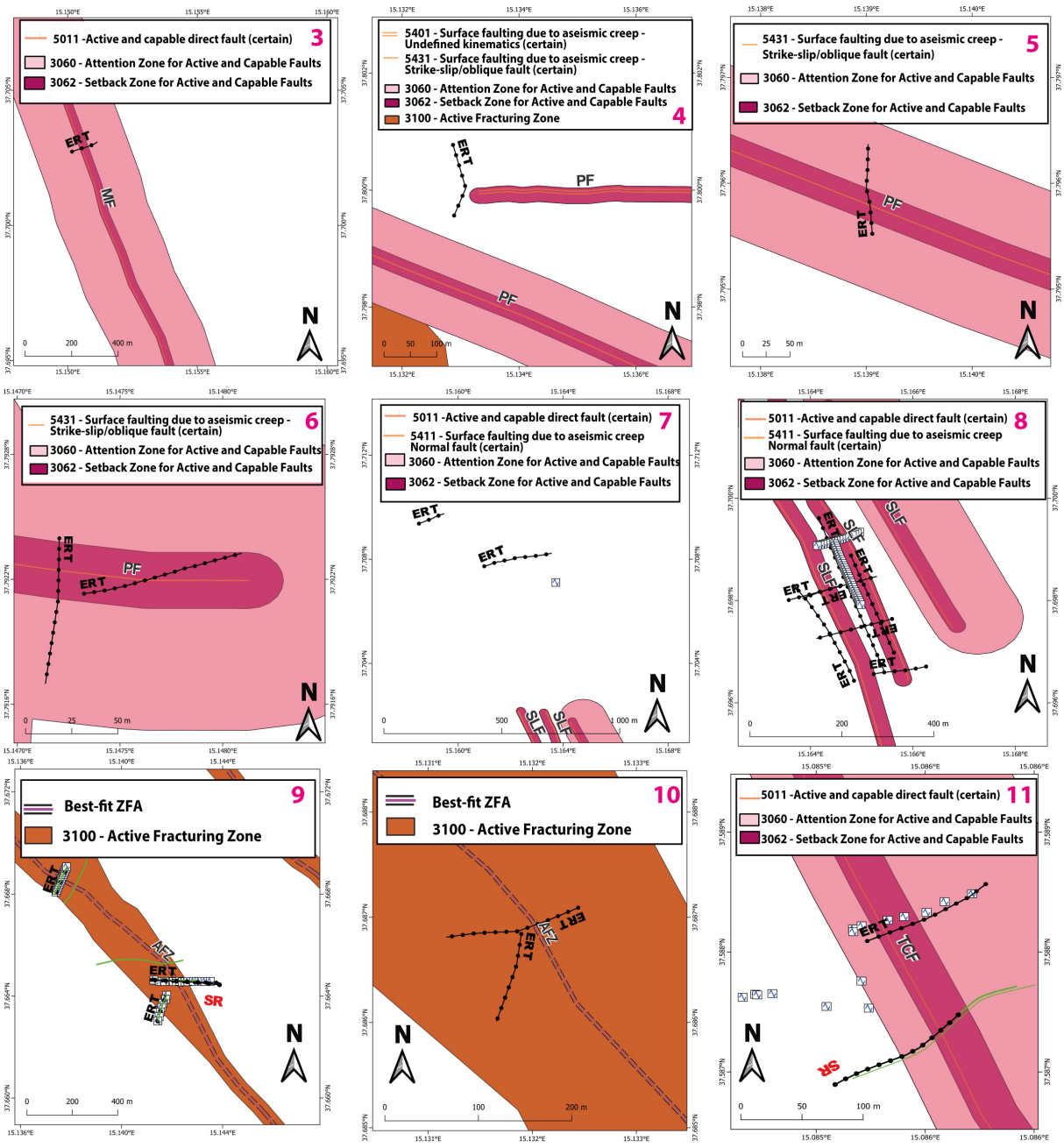

Figure 4 (continued). Details of the boxes 3-11 showing the location of the geophysical surveys. The numbers in the boxes correspond to the IDs listed in Table 3.

Figure 4 shows the sections of the investigated FAC while Table 3 lists the investigated FAC along with their corresponding reclassification and the type and number of geophysical surveys performed. Generally, depending on measurement logistics, various geophysical methodologies were employed, utilizing different levels of resolution where possible, as specified in Annex 1.

The following examples, extracted from the seven summary reports (Annex 1 in Gruppo di lavoro Fac Etna, 2024) highlighted the multidisciplinary approach adopted to characterize FAC in the Etnean region. Each site, in fact, illustrates the integration of five key pillars:

- Tectonic and Geodynamics: Defining fault kinematics, geometry, and their role within the regional framework (e.g., distinguishing between seismic slip and aseismic creep).
- Surface Manifestations: Identifying geomorphological markers such as fault scarps and ground deformations that reveal active tectonic signatures.

- Seismic History: Correlating historical and instrumental data to map the spatial and temporal distribution of events.
- State-of-the-Art Research: Grounding site-specific observations in a robust review of existing peer-reviewed literature.
- Applied Geophysics: Utilizing project-specific surveys and comparative data processing to visualize subsurface fault structures.

The selected cases demonstrate how the synergy of geological and geophysical data provides a comprehensive model for assessing active faulting and its territorial impact.

Table 3. List of investigated FAC segments and geophysical surveys.

Segment ID No.	Fault Name	Fault Code	Behavior Description of Investigated Segment	Segment Classification Type	Investigation Method and Number of Surveys
1	ZFA				31 HVSR; 1 SR; 1 GPR; 4 ERT
2	FAC_Fiandaca	FF	seismic; oblique-right	Certain	4 Ω mapper
3	FAC_Moscarello	MF	seismic; normal with right-lateral component	Certain	1 ERT
4	FAC_Pernicana	PF	creep; left-lateral strike-slip	Certain	1 ERT
5	FAC_Pernicana	PF,	creep; left-lateral strike-slip	Certain	1 Ω mapper
6	FAC_Pernicana	PF	Creep; left-lateral strike-slip	Certain	1 ERT; 1 Ω mapper
7	FAC_San Leonardello	SLF	seismic and seismic/creep; normal with right-lateral component	Certain	1 HVSR; 3 ERT
8	FAC_San Leonardello	SLF	creep; normal with right-lateral component	Certain	45 HVSR; 7 ERT
9	ZFA				35 HVSR; 1 SR; 5 GPR; 3 ERT
10	ZFA				2 Ω mapper
11	FAC_Trecastagni	TCF	seismic; right-lateral strike-slip/oblique	Certain	15 HVSR; 1 SR; 2 GPR; 1 ERT

4.1 The Fiandaca FAC

This example focuses on the Fiandaca Fault, a primary structural element within the Etnean tectonic framework. This site serves as a representative case for studying FAC evidence due to its well-documented history of both seismic slip and aseismic creep.

The structure exhibits a marked difference between its northern and southern sectors (Fig. 4). The northern sector of the structure is characterized by NW-SE and NNW-SSE striking fault zones exhibiting right-lateral normal motion. This kinematics is consistent with the broader strike-slip regime of the area and is associated with significant seismic activity (Azzaro et al., 2013). Conversely, the southern sector features several fault zones with similar right-lateral normal displacement but is primarily dominated by aseismic creep (Tringali et al., 2021).

The structural expression is closely tied to the local volcanic stratigraphy (Branca et al., 2011). In the northern sector, the structure intersects the volcanic products of the Filosofo Formation (122 BCE-1669 CE), while further south, it cuts through the older Pietracannone Formation (3.9 ka-122 BCE).

Observations following the December 26, 2018, earthquake (Mw 4.9) provided critical insights into how the age of these deposits dictates the spatial distribution of surface deformation (Civico et al., 2019; Romagnoli et al., 2021). Diffuse fracturing is observed where the fault plane is draped by recent lava flows (e.g., the 1030 CE flow), coseismic fracturing is distributed across an exceptionally broad zone, extending up to 500 m from the principal rupture axis (Tortorici et al., 2021). Localized displacement are present where the fault intercepts older protohistoric (3.9 ka) or Roman-age (122 BCE) flows, the primary fracturing resulted in clearly defined surface offsets (Azzaro, 1999). The structure was mobilized almost in its entirety, yielding a right-lateral displacement of 0.7 m. The resulting fracturing fields strictly correlated with the subsurface lithostratigraphy described above. Due to these characteristics, the northernmost sector (Segment 1), where a lack of distinct morphological evidence precludes the identification of a single principal fault plane, has been classified as an Active Fracturing Zone (ZFA). This designation is utilized to accurately represent the extensive and diffuse nature of coseismic phenomena in this specific volcanic-tectonic context (Tortorici et al., 2021; Tringali et al., 2021).

The study utilizes several techniques, including ERT, specifically using the Wenner configuration for comparative analysis, HVSR, GPR and seismic refraction/reflection (SR).

Segment 1 provides the most detailed dataset (Figs. 5-8). The ERT, HVSR, and GPR results characterize significant subsurface variability, but they do not reveal a unique geophysical anomaly that can be unambiguously associated with the mapped shallow fault trace. The ERT model nevertheless shows localized conductive anomalies, including one a few meters southwest of the mapped trace, which may indicate discrete zones of enhanced fracturing. These observations emphasize the need for integrated interpretation rather than fault identification based on a single geophysical attribute.

GPR analysis shows that the 100 MHz antenna was identified as the optimal tool for this site, while the 270 MHz antenna achieved high resolution in the upper layers but it suffered from rapid attenuation beyond a depth of 4-5 m. A test was performed also with the 40 MHz antenna but it was discarded due to insufficient resolution and an excessively large Fresnel zone, which caused unwanted spatial averaging.

Preliminary active seismic results indicate that the tomographic inversion is characterized by a high degree of smoothing. However, the reflection seismic processing of the same data (Fig. 6) demonstrates a high level of structural coherence with the GPR radargrams, validating the interpreted interfaces. The acquisition geometry adopted at this test site (5 m receiver spacing and 10 m source spacing) was constrained by field logistics and was not designed as the reference configuration for high-resolution shallow fault imaging. The relatively sparse source sampling limits ray redundancy and contributes to smoothing of the tomographic model. For dedicated FAC investigations, a denser source distribution is recommended; where feasible, source spacing should be no greater than approximately one-half of the receiver spacing.

In the present project the Ohm Mapper system was used as a complementary resistivity-mapping tool (Fig. 4). Compared with conventional multi-electrode ERT, the Ohm Mapper system allows rapid, non-invasive resistivity mapping without galvanic electrode contact, although its applicability and investigation characteristics depend on site conditions and it does not replace conventional ERT where detailed resistivity imaging and greater control of acquisition geometry are required. Since equipment availability and operational costs vary substantially among operators, this method is considered an optional complementary technique rather than a mandatory professional standard for FAC investigations.

In Segment 2 (Figs. 4 and 7a), the Ohm Mapper survey identified a resistivity anomaly (Fig. 7b). However, its correspondence with the mapped fault trace and its lateral extent remain uncertain. Similarly, in Segment 3 (Figs. 4 and 8a) the OHM Mapper/ERT survey identified a resistivity anomaly (Fig. 8b). As in Segment 2, additional data are required to confirm its correspondence with the mapped fault trace and to better constrain its lateral extent.

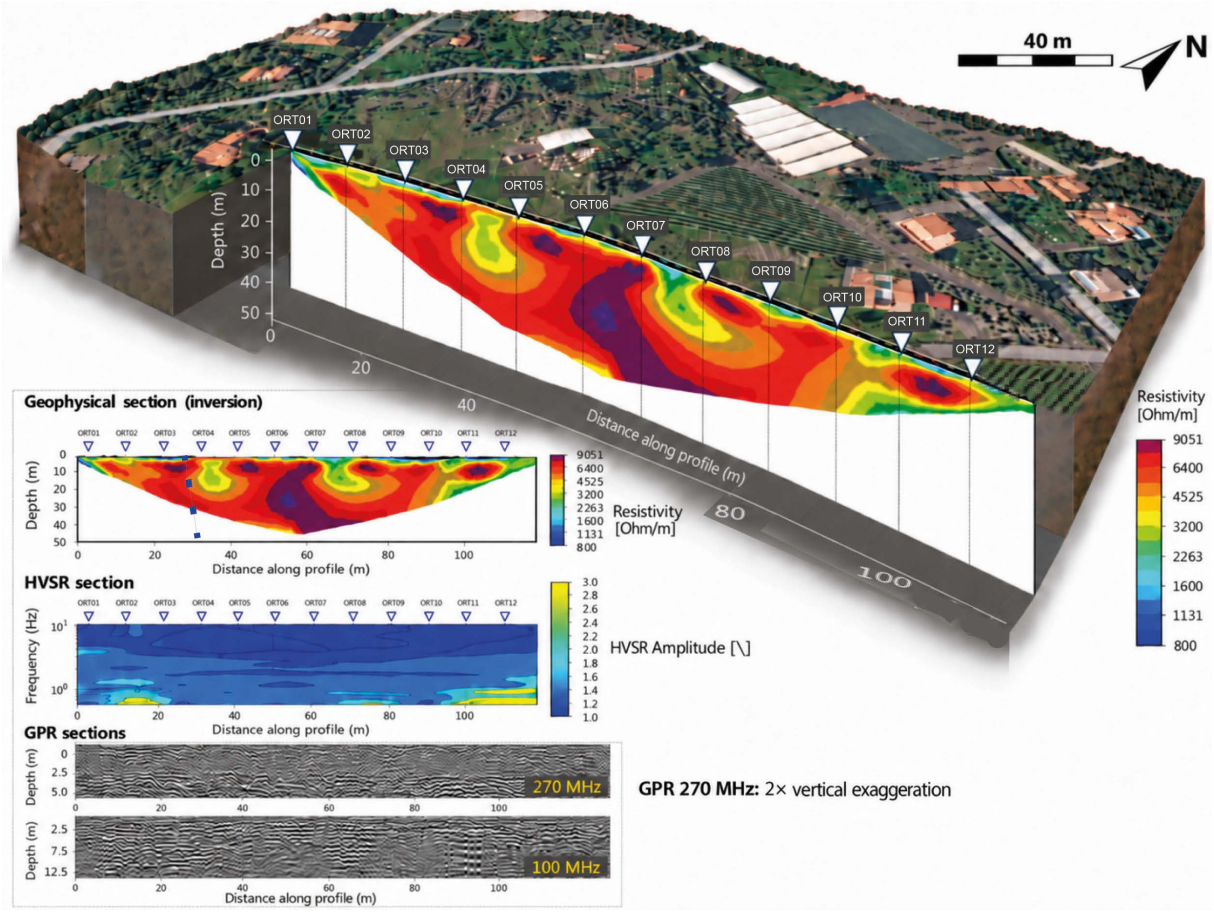

Figure 5. Aerial view of the geophysical Segment 1 (in Fig. 4) in the area Acireale-Fiandaca. Comparison between the geophysical surveys conducted at Segment 1 (the location shown in Fig. 4): (top) ERT model obtained using Wenner configuration; (middle) pseudo 2D interpolation of HVSR curves; (bottom) GPR profile acquired using respectively 270 MHz and 100 MHz antennas. The mapped trace of the Fiandaca Fault is shown by blue dashed line in the ERT Model.

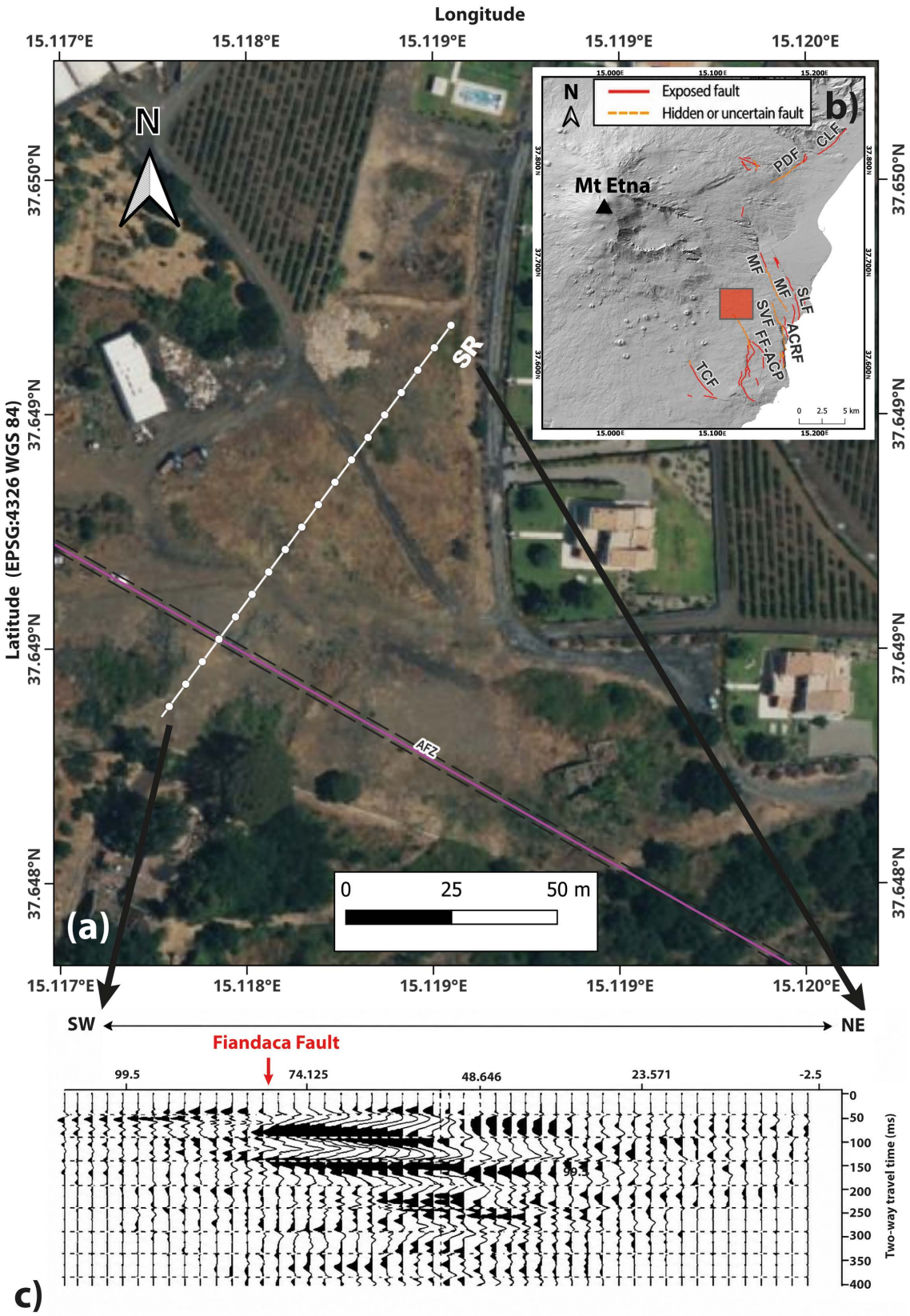

Figure 6. An example of seismic reflection surveys conducted in Segment 1 (the location is reported in Fig. 4). (a) Aerial view of the investigated area showing the mapped best-fit AFZ and the location of the seismic refraction/reflection (SR) profile. (b) Regional structural setting of the study area, with the main mapped fault systems; the red box indicates the location of the investigated site. (c) The data were acquired using seismic shotgun source with a source spacing of 10 m. Along the line were deployed 24 geophones with frequency 4.5 Hz spaced 5 m. The trace of the Fiandaca Fault is also shown (red arrow).

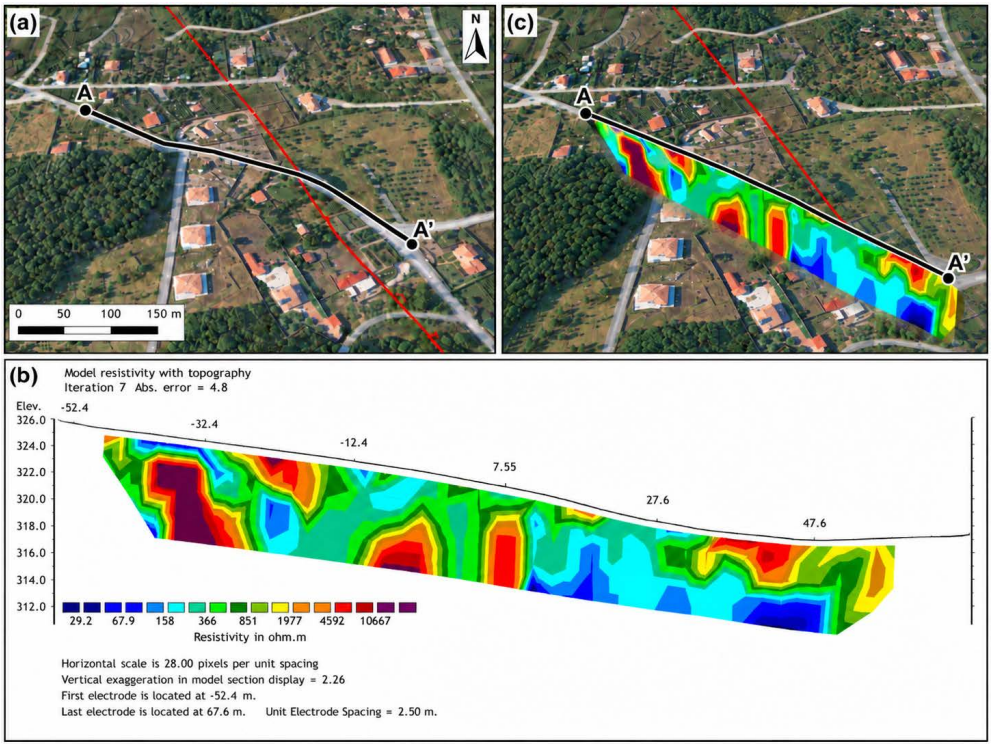

Figure 7. (a) Aerial view of the survey area showing the OhmMapper/ERT profile A-A′ and the mapped fault trace. (b) Three-dimensional view of the resistivity section positioned along the survey line, with the fault trace projected consistently with its mapped position in panel (a). (c) Inverted resistivity model with topography along profile A-A′; resistivity values are expressed in Ω·m. The same resistivity colour scale is used throughout the figure.

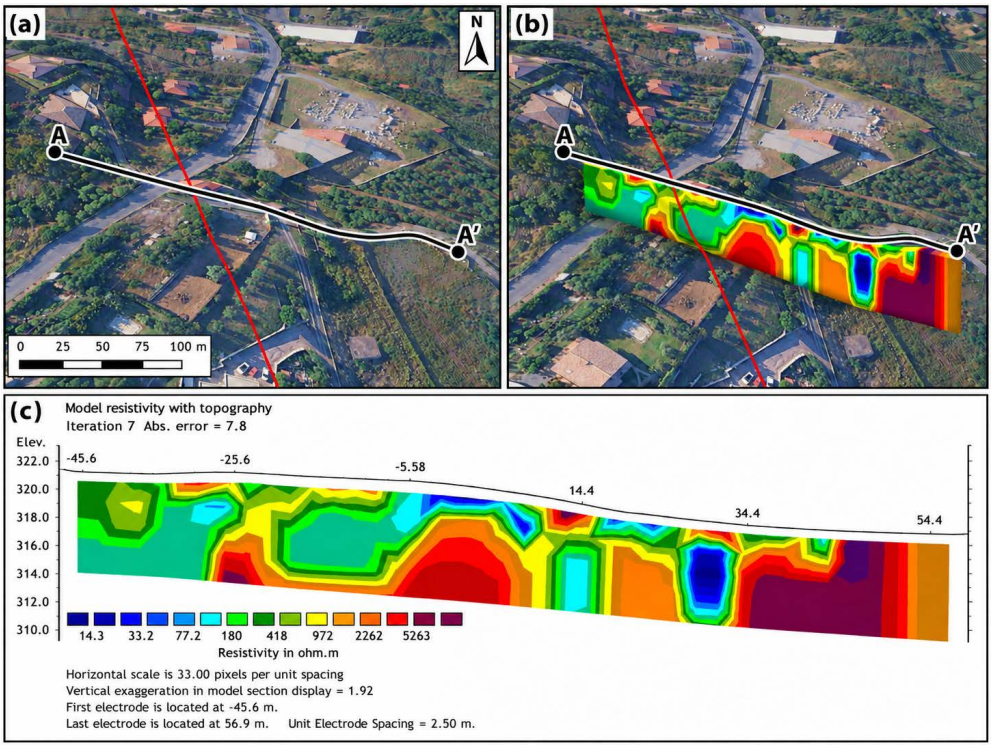

Figure 8. (a) Aerial view of the survey area showing the OhmMapper/ERT profile A-A′ and the mapped fault trace. (b) Three-dimensional view of the resistivity section positioned along the survey line, with the fault trace projected consistently with its mapped position in panel (a). (c) Inverted resistivity model with topography along profile A-A′; resistivity values are expressed in Ω·m. The same resistivity colour scale is used throughout the figure.

5. Conclusions

The extensive geophysical investigation carried out within the Etna FAC_MS Project has led to the formalization of robust protocols for the detection and characterization of Active and Capable Faults (FAC) in a complex volcanic environment. The integration of geological and multi-parametric geophysical data allows for the following detailed conclusions.

The study confirms that no single geophysical method is sufficient to fully characterize FAC in volcanic terrains. The combined use of ERT and GPR proved particularly valuable: ERT constrained lateral resistivity gradients and anomalous zones consistent with fault-related structures, while GPR provided high resolution constraints on near surface reflector geometry and deformation where penetration conditions were favorable. Seismic reflection provided complementary structural information consistent with the interpreted reflector geometry.

The marked lithological heterogeneity of Mt. Etna, characterized by alternating lava flows and volcanoclastic deposits, significantly impacts signal propagation and the geophysical response of fault-related structures. Our results show that acquisition geometry and array selection must be adapted to the target depth, expected physical-property contrasts, and local site conditions. The identification of Diffuse Fracture Zones (ZFA) and Aseismic Creep sectors highlights the need for high-density sampling to avoid the misinterpretation of localized volcanic features as tectonic lineaments.

The proposed protocols provide a structured framework for the application of geophysical investigations within Seismic Microzonation. By providing objective physical criteria to identify the “Surface Fault Rupture” (SFR) hazard, these guidelines enable the transition from broad “Areas of Attention” to better constrained Susceptibility (ZS) and Respect Zones (ZR). This high-resolution mapping is critical for mitigating risk in the densely populated slopes of Etna, where tectonic displacement can severely damage critical infrastructure and residential buildings.

The definition of four operational geophysical conceptual models (Exposed, Buried, Active Fracturing, and Creep) provides a standardized framework for future studies. These models serve as an “interpretative key” for professionals, reducing the subjectivity inherent in geophysical interpretation and ensuring that subsurface models are geologically consistent with the active kinematics of the volcano’s flanks.

In conclusion, the LG_FAC_Etna guidelines offer a repeatable workflow tested across representative Etnean fault settings. Future applications should aim to integrate these 2D protocols into 3D structural models to better understand the three-dimensional geometry of fault-related deformation zones. This approach not only enhances scientific knowledge of volcanic tectonics but also provides local authorities with a reliable tool for resilient urban planning and long-term risk reduction strategies.

Appendix A.

This chapter summarizes the acquisition, processing, and interpretation recommendations adopted for the geophysical characterization of Active and Capable Faults (FAC) in the Etnean volcanic environment. Only method-specific parameters relevant to the survey strategies discussed in the manuscript are reported; general theoretical aspects of the individual geophysical techniques are omitted. The protocols are adapted from Chapter 4 of the extended technical guidelines prepared by "Gruppo di lavoro Protocolli" and distributed by CMS (2020) and from Caielli et al. (2020).

Survey geometry, sensor spacing, and investigation depth must always be adapted to the expected dimensions of the fault-related structures, local geological conditions, accessibility, environmental noise, and the specific objectives of the investigation.

A.1 HVSR

A.1.1 Measurement Planning and Field Operations

- **Instrumentation**: Three-component velocimeters with natural frequency lower than the frequency range of interest, preferably <2 Hz, coupled with a signal digitizer with a dynamic range ≥16-bit. The use of accelerometers should be discouraged due to high noise levels and environmental interference
- **Sensor Coupling and Environmental Constraints**: The sensor should be stably coupled and levelled throughout the acquisition; any tilting may induce artefacts in the H/V spectral ratio. Measurements on high-impedance artificial surfaces (e.g., asphalt or concrete) overlying compliant layers should be avoided, as near-surface velocity inversions may attenuate the fundamental H/V peak (Castellaro and Mulargia, 2009). Following SESAME (2004) guidelines, measurements must be conducted under favourable weather conditions, specifically, without rain and with wind speeds below 5 m/s.
- **Acquisition Parameters**: To ensure a statistically representative characterization of the ambient vibration field, the recording duration of at least 20-30 minutes is suggested, with a sampling frequency >100 Hz. Longer durations are recommended for sites with high noise levels.
- **Site Geometry and Free-Field Conditions**: To mitigate the influence of structural oscillations or building-induced noise, a minimum distance of 15 m from civil structures is required. This threshold ensures free-field conditions, consistent with the findings of Castellaro and Mulargia (2010), who identified the boundary of structural influence at approximately 12 m.
- **Sensor Alignment**: The sensor must be oriented toward geographic North.
- **Pseudo-2D Profiling and Spatial Arrays**: HVSR measurements performed along linear profiles or arrays allow the reconstruction of Pseudo-2D sub-surface models. Data should be acquired using seismic nodes or individual mobile three component stations (preferably with simultaneous acquisition). Transects must be of sufficient length to cover the area of interest (minimum 60 m), with a sensor spacing of 5-10 m (Famiani et al., 2022).

A.1.2 Data Processing and Interpretation

Given the significant impact of post-processing procedures on H/V spectral ratio values, it is recommended to adopt homogeneous analysis methods (smoothing, windowing, transient removal, etc.) to ensure the effective comparability of results obtained within the same area. Specifically, the following recommendations are provided:

- **Window Selection and Transient Removal**: Selection of time windows should be performed using an STA/LTA (Short-Term Average/Long-Term Average) transient filter (e.g., short window: 1 s; long window: 25 s; STA/LTA threshold = 2.5) or manually. Transient removal must be carried out with caution, evaluating its potential impact on the analysis results. When amplitude spectra are calculated using a stacking method of values obtained from sub-windows of the sampled series, a time duration of 25-30 seconds is suggested for each window. In any case, the total number of windows considered for the final estimate (after any transient removal) should not be less than 20.

- **Filtering**: No filters should be applied.
- **Tapering**: 5% cosine taper with no time-window overlap.
- **Component Averaging**: Quadratic mean of the horizontal components N(f) and E(f). Other types of averaging, such as the geometric mean, are appropriate if a significant difference is observed between the components.
- **Smoothing**: Use of spectral smoothing procedures on moving windows with frequency-dependent bandwidth (e.g., Konno-Ohmachi with b = 40, or triangular windows with a width equal to 5% of the central frequency, etc.).
- **Frequency Range**: Processing must ensure spectral value estimates within the 0.2-20 Hz frequency range, with approximately 200 values equally spaced on a logarithmic scale.
- **Directionality Analysis**: HVSR directionality analysis to evaluate the polarization of the noise source.
- **Quality Control**: A quality analysis should be performed according to the criteria reported in the "Contributions for the update of Guidelines and Criteria for Seismic Microzonation" (AA.VV., 2011) repeating measurements when necessary.
- **Pseudo-2D HVSR Analysis**: The processing of data acquired through the Pseudo-2D HVSR method follows the same procedures adopted for the single-station processing described above.

A.1.3 Data and Results Transfer

Minimum deliverables should include:

- **Metadata**: Each HVSR measurement must be accompanied by an HVSR Acquisition Field Sheet in text format (survey metadata sheet).
- **Methodology**: A description of the post-processing procedures adopted.
- **Digital Output**: An ASCII digital file for each frequency containing:
  Mean spectral ratio values.
  Maximum and minimum values and/or the relative confidence interval.
  Fundamental frequency value (f_0) and the corresponding peak amplitude (A_0)
- **Original Data**: Raw data and a file in ASCII or another standard seismological format (e.g., SAC, SAF, miniSEED, etc.).
- **Pseudo-2D HVSR Results**: The results will consist of cross-sections generated by interpolating individual HVSR measurements taken at various points along the survey line. The output will be a distance-frequency section where the attribute is the HVSR amplitude.

A.1.4 Recommendations specific to the Etnean volcanic environment

To better evaluate potential effects related to geological or volcanological characteristics on the recordings, it is strongly recommended to constrain measurement stations to sites where geological and stratigraphic information is well-established and accurately documented.

A.2 Refraction and MASW

A.2.1 Measurement Planning and Field Operations

Acquisition parameters and geometry depend on the signal sampling in both time and space (wavefield), the minimum and maximum investigation depths, and the seismic survey layout.

Wavefield Sampling

Wavefield sampling depends on the source signal spectrum (its maximum frequency, f_{max}) and the phase velocity of the ground (its minimum velocity, V_{min}). Signals must be sampled in the time domain with a sampling frequency (fs) greater than $2f_{max}$, and spatially with a geophone spacing of less than $V_{min}/2f_{max}$.

Oversampling in both time and space is always recommended to reduce errors in picking arrival times and to better reconstruct the velocity spectrum in the F-K (frequency-wavenumber) or F-slowness domains.

Maximum and Minimum Investigation Depth

- **Refraction**: Maximum depth is approximately 1/4 of the total profile length; minimum layer depth is approximately 1/2 of the geophone spacing.
- **MASW**: The maximum investigation depth is approximately $Z_{max} \leq VR/(2F_{min})$, while the minimum layer depth is approximately $Z_{min} \geq VR/(2F_{max})$ where F_{min} and F_{max} are the minimum and maximum frequencies of the signal spectrum, respectively, and VR is the average Rayleigh wave phase velocity. It is suggested to simultaneously acquire MASW and P-wave refraction data using the same instrumentation and survey geometry.

Technical Specifications for Data Acquisition

- **Instrumentation**: Digital seismographs with a dynamic range >20 bit, at least 24 channels, and vertical geophones with a natural frequency ≤4.5 Hz.
- **Recording Duration**: Sufficient to capture the entire useful signal (indicatively ≥2 s) with a sampling frequency ≥512 Hz.
- **Trigger**: The source must be triggered with an error ≤1 ms.
- **Source**: Sledgehammer with a recommended mass of 8-10 kg.
- **Quality and Stacking**: To ensure optimal data quality, records from different impacts must be acquired separately (single shots) or through manual signal stacking depending on background noise.

MASW Specifics

- **Data** must be acquired and stored individually after each impact without any in-field signal stacking.
- **Filtering**: Data must be recorded without applying filters.
- **Geophone Spacing**: Should not exceed 3 m (for long MASW-1D or refraction surveys, a larger spacing, such as 5 m, may be used).
- **Minimum Number of Shots** (P-wave and MASW-1D): 3 internal shots (1 at the center, 1 at 1/4, and 1 at 3/4 of the spread). 2 end-of-line shots (start and end of the spread). 2 far shots with a minimum offset of 1/4 of the spread (also for MASW). 2 far shots with a minimum offset of 1/2 of the spread (also for MASW).
- **HVSR Integration**: At least one HVSR measurement along the profile (recommended in the central part).
- **Topography**: The recording surface should not have high roughness, with elevation differences ≤1/4 of the geophone spacing and a local slope not exceeding 15°.
- **Redundancy**: To acquire redundant data for MASW-1D analysis, acquisition can be integrated with external shots at 4-6 m from the ends of the spread.
- **Avoid Bias**: To prevent underestimating or overestimating P-wave and Rayleigh wave phase velocities (apparent velocities), sources should be located to ensure subsurface sampling from different directions.
- **Pseudo-2D MASW**: To reconstruct Pseudo-2D velocity models using the MASW-1D technique, roll-along configuration acquisitions shall be performed. Shots are carried out externally to the geophone spread, moving the spread along the survey line for each shot. The source will be positioned at the end of the spread with first-geophone offsets as previously described for MASW-1D (Park et al., 2007; Imposa et al., 2015).

S-wave Refraction

For S-wave refraction, all previously described parameters apply, with the following differences:

- **Geophones**: Horizontal geophones with a natural frequency ≥4.5 Hz (or specific S-refraction geophones ≥10 Hz), all oriented in the same direction and perpendicular to the survey line.
- **Source**: Horizontal impact system on a beam or block coupled to the ground. The sequence includes a P-wave impact (vertical), followed by S+ and S– impacts (transverse impacts in both directions perpendicular to the survey line).
- **Record Length**: Window length ≥1 s.

A.2.2 Data Processing and interpretation

P-wave and S-wave Refraction Processing

- **Acquisition geometry input**, editing, and removal of traces characterized by high noise levels.
- **Spectral analysis**.

- **Preprocessing** consisting of filtering and first-arrival picking. It is recommended to perform first-arrival picking on unfiltered data and subsequently verify them against filtered data; furthermore, reciprocal times for shots in reciprocal configurations must be checked.
- **1D interpretation**, for example, using the intercept time method from first-arrival picks related to reciprocal sources.
- **2D interpretation**, for example, using the intercept time method, the delay-time method, or GRM (Generalized Reciprocal Method) from first-arrival picks related to reciprocal sources. Error/uncertainty values for the depths and velocities of horizons/interfaces must be provided.
- **Tomographic inversion** from first-arrival times for all sources. Hit-counts (ray coverage) for each velocity value and the corresponding error/uncertainty must be provided.

Interface-based refraction interpretations may constrain discrete velocity boundaries, whereas tomographic inversion reconstructs smooth lateral and vertical variations in the velocity field. These two types of interpretation should therefore be integrated with appropriate consideration of their different resolution and assumptions.

MASW Processing

The processing of acquired data must be preceded by a pre-processing phase in which traces with the highest noise levels are removed. The following steps will then be performed:

- **Calculation of Rayleigh wave velocity/slowness spectra** (frequency range 5-50 Hz).
- **Summation of velocity spectra** in reciprocal configurations.
- Based on the Rayleigh wave phase velocity (VR) values, an **evaluation of the maximum investigation depth** $h_{max} = VR/(2f_{min})$ and the minimum depth of surface layers $h_{min} = VR/(2f_{max})$, as a function of the minimum and maximum frequencies considered (f_{min} and f_{max} respectively).
- **Selection of the dispersion curve** to identify the fundamental mode and any higher modes from the Rayleigh velocity (or slowness) spectra.

A.2.3 Data and Results Transfer

MASW and P/S-wave Refraction

- **Field sheets** for Refraction/MASW measurements for each spread in text format (Survey Metadata Sheet).
- **Original raw data** in ASCII or other standard seismological formats (e.g., SAC, SEG-Y, SEG2, etc.).

Deliverables for P and/or S-wave Refraction

- **First-arrival picking files** for each source.
- **1D Model** files showing the depth of the layer top, relative P and/or S velocity, seismic-stratigraphic unit assignment, and uncertainty.
- **2D Model** files reporting, for each identified interface, the metric coordinate along the profile, depth, and P and/or S velocity of the layer, seismic-stratigraphic unit assignment, and uncertainty.
- **Tomographic model** files reporting the coordinates (x, z) of the velocity pixels and the corresponding P-velocity value (x: metric coordinates along the spread; z: depth). Assignment of seismic-stratigraphic units to P and/or S velocity intervals.

Deliverables for MASW

- **Phase velocity or slowness spectrum**.
- **Dispersion curve picking values**.
- **1D Model** file showing the depth of the layer top, corresponding S-velocity, uncertainty, and seismic-stratigraphic unit assignment. This file integrates the P-velocity model file.
- **Pseudo-2D MASW Model**, consisting of the interpolation of 1D velocity-depth models obtained as described above and positioned at their respective locations.

A.2.4 Recommendations specific to the Etnean volcanic environment

Numerical inversion procedures must be applied to determine the Vs profiles for each dispersion curve measurement. Due to the mathematical complexity of the physical model relating subsurface characteristics to the dispersion curve, inversion procedures assume the subsurface is characterized by a vertical succession of homogeneous plane-parallel layers (1D model); therefore, they can only be applied in such subsurface configurations. Furthermore, even in simple 1D situations, the forward problem model is characterized by marked non-linearity, which produces significant ambiguity in the inverse problem solutions. In such cases, exploratory or global-search inversion procedures (e.g., Genetic Algorithms) may be preferable to local gradient-based methods, particularly where strong non-linearity and non-uniqueness are expected. Local gradient-based methods may be strongly influenced by the choice of the initial model and may therefore explore the solution space only locally. It should be emphasized that many seismic-stratigraphic configurations may remain compatible with the observed data.

To reduce the ambiguity of the inverse problem solution, additional constraints must be introduced. In particular, the geological model plays a primary role in constraining the range of admissible layer thicknesses and Vs values.

Independent Measurements: Results from gravity surveys, resistivity, or Vp profiles (including P-wave first arrivals deducible from MASW recordings) are strongly encouraged.

HVSR Curves: These can be inverted alone, but results have even higher ambiguity than dispersion curves. For Vs profile determination, joint inversion procedures (exploratory type) should be used.

Before using advanced codes, it is advisable to conduct rapid, approximate (and thus more robust) analyses by examining experimental data via charts, simplified models (power laws), or representations of dispersion curves as phase velocity relative to wavelength.

A.3 Electrical Resistivity Tomography (ERT)

A.3.1 Measurement Planning and Field Operations

The location and orientation of 2D ERT profiles must be defined on the basis of a preliminary geological-structural model of the target FAC. Whenever logistics permit, profiles should be oriented perpendicular to the expected strike of the fault or fracture zone.

Each profile must be accurately georeferenced and plotted on an appropriate scale. In areas of complex morphology, a detailed topographic survey must be performed to provide topographic corrections for the inversion models.

Before starting the resistivity measurements, background electrical noise must be evaluated particularly in urbanized areas and near power lines or industrial facilities. Contact resistance between the steel or copper electrodes and the ground must be systematically measured and recorded. When contact resistance is high (common on dry lava surfaces or asphalt), contact improving materials (e.g salt water, bentonite or conductive gels) should be used. In urban or high-value historical/architectural areas with stone paving, non-invasive metal plates may be used instead of driven electrodes.

Instrumentation requirements for 2D ERT: A digital multi-electrode resistivimeter capable of managing at least 48 electrodes. Minimum technical specifications are:

- Voltage measurement sensitivity ≤1 mV and current intensity measurement sensitivity ≤1 mA;
- Measurement of self-potential (SP) and electrode contact resistance;
- Ability to inject direct current (DC) into the subsoil with automatic polarity reversal at operator-defined time cycles, with a maximum current intensity of at least 2A;
- Automated stacking of apparent resistivity measurements with a relative standard deviation ≤5%;
- Automatic switching system allowing electrodes to be used both for current injection and voltage measurement;
- Output of an ASCII containing for each measurement: electrode positions, apparent resistivity value, injected current intensity, measured voltage, and standard deviation.

Data Acquisition

- Measurements should be performed using different electrode arrays (e.g., Wenner, Wenner-Schlumberger, Dipole-Dipole, etc.). The choice of array and electrode spacing must be optimized, according to the target

investigation depth and the spatial resolution required to detect lateral resistivity gradients associated with fault zone;
- For a maximum investigation depth of approximately 40-50 m, at least one profile must be acquired with ≥48 electrodes and an inter-electrode spacing of 5 m. For higher near-surface resolution, denser spacing (1-2.5 m) or combined variable spacing (roll-along) configurations are recommended.

A.3.2 Data Processing and Interpretation

- Processing apparent resistivity data includes the construction of 2D pseudosections, removal of outliers, and, where appropriate, the application of statistical filtering techniques;
- The estimation of the true 2D resistivity distribution must be performed by tomographic inversion using state of the art algorithms (commercial or open-source);
- Topography must be incorporated into the inversion. A quantitative assessment of inversion quality (RMS error or equivalent) must always be reported;
- In the volcanic setting of Mount Etna, particular attention should be paid to high lateral resistivity gradients and anomalous resistivity zones. These features may represent fault-related geophysical signatures and may be used to constrain the location and extent of fault or damage zones when supported by independent geological or geomorphological evidence. Their apparent width is controlled by acquisition geometry, effective spatial resolution, and inversion regularization and should not be interpreted as the true geological thickness of the fault zone;
- All processing and interpretation steps must be documented in a Technical Report (a digitally signed PDF prepared by the survey supervisor).

A.3.3 Data and Results Transfer

For each 2D ERT profile the following minimum deliverables are required to ensure uniformity and traceability according to Civil Protection Department standards:
- Field sheets containing:
  Operator name.
  Instrumentation used, electrode array type, number of electrodes, electrode spacing, number of stacks and full georeferencing of all electrode positions (shapefiles in WGS84EPSG:4326);
- **Raw Data**: ASCII file with electrode configuration, positions, current intensity, measured voltage, self-potential, apparent resistivity, standard deviation, and contact resistance (one row per measurement);
- **Image of the 2D apparent resistivity pseudosection** (JPG, TIFF, or PNG);
- **ASCII file of the inverted 2D Resistivity Model** (three-column table: distance along the profile, depth from ground surface, resistivity in Ω*m including the name of the inversion software;
- **Digitally signed PDF Technical Report**.

A.3.4 Recommendations specific to the Etnean volcanic environment

Given the logistical constraints of densely urbanized areas on the flanks of Mount Etna, particular care is recommended in electrode placement to ensure good electrical contact while minimizing damage to roads, pavements or structures of architectural value.

Because of the high level of electromagnetic noise typical of the Etnean area, the use of robust signal filtering systems and stacking procedures is strongly recommended.

To increase spatial resolution in the central part of the profile (where the FAC is expected) variable electrode spacing (e.g., 1-2 m in the central sector and 5 m at the ends) and roll-along acquisition techniques should be adopted whenever possible.

Additional electrode arrays (e.g., pole-dipole, multi-gradient) and reciprocal measurements are recommended to increase data quality, resolution and investigation depth, and to allow quantitative assessment of data reliability.

In highly heterogeneous volcanic sequences, the joint interpretation of ERT results with GPR, seismic and HVSR data is essential to reduce ambiguity in the identification of fault-related resistivity anomalies.

A.4 Ground Penetrating Radar (GPR)

A.4.1 Measurement Planning and Field Operations

The penetration depth and vertical resolution of Ground Penetrating Radar (GPR) surveys are primarily governed by the central frequency of the transmitted radar pulse. Commercial GPR antennas typically operate within a frequency range of 10-2000 MHz.

There is an inherent trade-off between penetration depth and resolution: lower frequencies allow greater penetration at the expense of spatial resolution, whereas higher frequencies provide higher resolution but are limited to shallower depths. Effective penetration depth is highly site-specific and depends on lithology, porosity, moisture content, alteration, and subsurface heterogeneity, which may significantly influence electromagnetic attenuation and scattering.

Data acquisition

Data acquisition can be performed in two distinct modes:

- **Time Mode**: The system triggers pulses at a constant time interval.
- **Distance Mode**: Triggers pulses at fixed spatial intervals, translating the antenna's movement into linear distance.

In both cases, the resulting two-dimensional profiles (radargrams) consist of a dense sequence of reflections.

For FAC investigations, profile orientation should be defined according to the expected geometry of the fault or deformation zone. Whenever possible, profiles should be oriented approximately perpendicular to the expected fault strike and acquired along the same transects used for other geophysical techniques.

Profiles should be accurately georeferenced, and surface elements that may generate radar anomalies or interpretation ambiguities should be mapped during acquisition.

Antenna frequency must be selected according to the expected target depth, required spatial resolution, and local electromagnetic conditions. Nominal penetration depths should therefore be considered indicative rather than fixed values, particularly in heterogeneous volcanic deposits.

Indicative frequency ranges and expected penetration/resolution values are reported below.

Antenna Frequency	Indicative Penetration Depth	Approximate Vertical Resolution
50 MHz	15-30+ meters	~0.5-1.0 meters
100 MHz	10-20 meters	~0.25-0.5 meters
200 MHz	5-10 meters	~0.1-0.25 meters

Minimum Technical Specifications

To ensure adequate data acquisition, the GPR system should allow:

- **Data Format**: Standard SEGY.
- **Scan Rate**: At least 50 scans/s.
- **Samples per Scan**: At least 512.
- **Sample Size**: 8 bit.
- **Gain Functions**: 1-5 points (−20 to +80 dB), manual or automatic.
- **Filters**: Vertical (Low-pass and High-pass IIR/FIR); Horizontal (Stacking, Background Removal).

Acquisition Parameters

The acquisition time window must be selected according to the expected maximum investigation depth and the estimated minimum propagation velocity, with an appropriate safety margin.

Temporal sampling must satisfy the Nyquist criterion with respect to the highest useful frequency of the recorded signal.

Spatial sampling must also be sufficiently dense to avoid aliasing and to adequately reconstruct reflector geometry.

A.4.2 Data Processing and Interpretation

Post-acquisition processing should be adapted to data quality and survey objectives. Processing should improve signal quality and reflector continuity without introducing artificial features into the radargrams.

Standard Processing sequence may include:

- **Orientation and Coordinates**: Correction of profile orientation and assignment of coordinates.
- **Zero-Time Correction**: Identification of the ground surface contact point and elimination of the "air wave."
- **Dewow Filtering**: Removal of low-frequency signals induced by the GPR system.
- **Background Removal**: Application of 2D filters to suppress horizontal signals and emphasize hyperbolic reflections (discontinuities).
- **Gain Application**: Using gain operators to emphasize low-amplitude signals.
- **Band-pass Filtering**: Frequency filtering centred on the peak frequency to suppress noise.
- **Hyperbola Analysis**: Calculation of propagation velocity and conversion of radargrams to depth functions.

Advanced/Optional Processes may include:

- **Deconvolution**: To increase frequency content (vertical resolution) and attenuate multiples/reverberations.
- **Migration**: Collapsing diffraction hyperbolas and correcting the angle of dipping reflectors.

For FAC characterization, interpretation should focus on spatially coherent variations in reflector geometry, including reflector offsets, terminations, changes in dip, localized disruption, diffractions, and anomalous scattering.

These features should not be interpreted as direct images of a discrete fault plane. Their significance as fault-related geophysical evidence should instead be evaluated together with geological, geomorphological, and other geophysical information.

All processing steps and parameters should be documented, and the final interpretation should be checked against the raw or minimally processed radargrams.

A.4.3 Data and Results Transfer

For each GPR profile, the following minimum information and products should be provided:

- Field acquisition sheet with description of instrumentation and antenna frequency, acquisition mode and spatial sampling, profile geometry and coordinates;
- RAW and final processed profiles in SGY format or equivalent standard format. Include migrated sections if applicable. The SGY Header must contain all geometry, acquisition parameters, and coordinates.
- Interpreted profiles indicating detected elements.
- Technical report describing acquisition, processing, and interpretation phases.

A.4.4 Recommendations specific to the Etnean volcanic environment

In the Etnean volcanic environment, the strong lithological and structural heterogeneity of lava flows and volcanoclastic deposits may cause significant electromagnetic attenuation and scattering. Consequently, effective penetration depth may be substantially lower than the nominal values expected from antenna frequency alone.

Antenna frequency should therefore be selected according to site conditions and investigation objectives:

- 100 MHz antennas: generally, provide a suitable compromise between penetration depth and spatial resolution for FAC investigations;
- 200-270 MHz antennas: provide higher resolution in the shallow subsurface but may suffer strong attenuation below only a few metres;
- 40-50 MHz antennas: may provide greater penetration but lower spatial resolution and a larger Fresnel zone, potentially limiting their effectiveness for narrow fault-related targets.

At the Fiandaca site, the 270 MHz antenna provided high resolution in the shallow subsurface but showed rapid attenuation below approximately 4-5 m, whereas the 40 MHz antenna was discarded because of insufficient resolution

and excessive spatial averaging. The 100 MHz antenna therefore represented the most suitable compromise for that specific site.

The absence of a clear GPR anomaly should not be considered evidence for the absence of a FAC, particularly where deformation is distributed, dielectric contrasts are weak, or electromagnetic attenuation is strong. GPR results should therefore be interpreted jointly with geological, geomorphological, ERT, seismic, and HVSR information.

Acknowledgements. This work was funded by the "Etna FAC_SM Project" through a collaboration agreement between the Civil Protection Department of the Sicily Region (DRPC Sicilia) and the CNR-IGAG/CentroMS. The authors acknowledge the entire ETNA FAC Working Group who contributed to data acquisition. We sincerely thank the Editor and the Reviewers for their thoughtful and constructive comments, which greatly contributed to improving the quality and clarity of the manuscript.

References

Annan, A. P. and S. W. Cosway (1994). GPR Frequency Selection: Proceedings of the Fifth International Conference on Ground-Penetrating Radar, Kitchener, Ontario, Canada, June 12-16, 1994, 747-760.

Azzaro, R. (1999). Earthquake surface faulting at Mount Etna volcano (Sicily) and implications for active tectonics. J. Geodynamics, 28, 193-213.

Azzaro, R., S. Branca, K. Gwinner and M. Coltelli (2012). The volcano-tectonic map of Etna volcano, 1:100.000 scale: morphotectonic analysis from high-resolution DEM integrated with geologic, active faulting and seismotectonic data, It. J. Geosciences (Boll. Soc. Geol. It.), 131, 1, 153-170.

Azzaro, R., A. Bonforte, S. Branca and F. Guglielmino (2013). Geometry and kinematics of the fault systems controlling the unstable flank of Etna volcano (Sicily). J. Volcanol. Geoth. Res., 251, 5-15.

Azzaro, R., A. Bonforte, S. D'Amico, F. Guglielmino and L. Scarfì (2020). Stick-slip vs. stable sliding fault behavior: a case-study using a multidisciplinary approach in the volcanic region of Mt. Etna (Italy). Tectonophysics, 790, 228554, doi:10.1016/j.tecto.2020.228554.

Azzaro, R., S. Pucci, F. Villani, R. Civico, S. Branca et al. (2022). Surface faulting of the 26 December 2018, M_w5 Mt. Etna earthquake (Italy): geological source model and implications for the seismic potential of the Fiandaca fault, Tectonics, 41, doi:10.1029/2021TC007182.

Binley, A. and L. Slater (2020). Resistivity and Induced Polarization Theory and Applications to the Near-Surface Earth. by, Cambridge University Press, 388.

Bonforte, A., F. Guglielmino and G. Puglisi (2013). Interaction between magma intrusion and village-scale axial faulting revealed by joint use of InSAR and GPS data: The case of the 2001 Mt. Etna eruption, J. Geodyn., 67, 40-46.

Branca, S., M. Coltelli and G. Groppelli (Ed.) (2015). Carta Geologica del Vulcano Etna. ISPRA-Servizio Geologico d'Italia, Mem Descr. Carta Geol. Italia, XCVIII, 180 pp., 2 App., 1 carta a scala 1:50.000.

Branca, S., M. Coltelli, G. Groppelli and F. Lentini (2011). Geological map of Etna volcano, 1:50,000 scale. It. J. Geosci. (Boll. Soc. Geo. It.), 130 (3), 265-291.

Caielli, G., R. de Franco, V. Di Fiore, D. Albarello et al. (2020). Extensive surface geophysical prospecting for seismic microzonation, Bull. Earthq. Engin., doi:10.1007/s10518-020-00866-4.

Castellaro, S. and F. Mulargia (2009). The effect of velocity inversions on H/V, Pure Appl. Geophys., 166, 4, 567-592, doi:10.1007/s00024-009-0474-5.

Castellaro, S. and F. Mulargia (2010). How far from a building does the ground-motion free-field start? The cases of three famous towers and a modern building, Bull. Seismol. Soc. Am., 100, 5A, 2080-2094, doi:10.1785/0120090188.

Civico, R., S. Pucci, R. Nappi, R. Azzaro, F. Villani et al. (2019). Surface ruptures following the 26 December 2018, Mw 4.9, Mt. Etna earthquake, Sicily (Italy), J. Maps, 15, 831-837, doi:10.1080/17445647.2019.1683476.

De Beni, E., S. Branca, M. Coltelli, G. Groppelli and J. Wijbrans (2011). 39Ar/40Ar isotopic dating of Etna volcanic succession, Ital. J. Geosci., 130, 3, 292-305.

Dolce, M., S. Castenetto et al. (2011). Contributi per l'aggiornamento degli "Indirizzi e criteri per la microzonazione sismica" Supplemento alla Rivista n. 2-2011 Anno XXVIII, Pàtron Editore, Bologna (disponibile all'indirizzo https://www.protezionecivile.gov.it/it/pubblicazione/contributi-laggiornamento-degli-indirizzi-e-criteri-la-microzonazione-sismica/).

Famiani, D., F. Cara, G. Di Giulio, M. Vassallo and G. Milana. (2022). Detection of hidden faults within the Fucino basin from single station ambient noise measurements: The case study of the Trasacco fault system., Front. Earth Sci., 19, doi:10.3389/feart.2022.937848.

Gambino, S., A. Bonforte, A. Carnazzo, G. Falzone et al. (2011). Displacement across the Trecastagni Fault (Mt. Etna) and induced seismicity: the October 2009 to January 2010 episode. Annals of Geophysics 54 (4), 414-423.

Gruppo di lavoro ETNA FAC (2024). Linee Guida per lo studio delle Faglie Attive e Capaci (FAC) nell'area vulcanica etnea. Versione 1.0. Accordo ai sensi dell'art. 15 della legge 241/1990 e del decreto legislativo 50/2016 e ss.mm.ii. tra il Dipartimento Regionale della Protezione Civile della Presidenza della Regione Siciliana e il CNR Istituto di Geologia Ambientale e Geoingegneria, CUP: B75F21002880002, 242.

Gruppo di lavoro Protocolli di acquisizione ed elaborazione dati relativi alle attività di Microzonazione Sismica di livello 3 in Italia Centrale (2020). ISBN 978 88 8080 408 6, Cnr Edizioni, 2020, Roma, https://www.centromicrozonazionesismica.it/documents/33/Protocolli_di_acquisizione_ed_elaborazione_dati_di_MS_di_livello_3_in_Italia_Centrale.pdf.

Imposa, S., G. De Guidi, S. Grassi, S. Scudero et al. (2015). Applying geophysical techniques to investigate a segment of a creeping fault in the urban area of San Gregorio di Catania, southern flank of Mt. Etna (Sicily – Italy), J. Appl. Geoph. 123, 153-163, doi:10.1016/j.jappgeo.2015.10.008.

ITHACA Working Group (2019). ITHACA (ITaly HAzard from CApable faulting), A database of active capable faults of the Italian territory, Version December 2019, https://www.isprambiente.gov.it/en/projects/soil-and-territory/italy-hazards-from-capable-faulting.

Linee Guida FAC (2015). Linee guida per la gestione del territorio in aree interessate da Faglie Attive e Capaci (FAC). Versione 1.0. Commissione tecnica per la Microzonazione sismica, Conferenza delle Regioni e Province autonome – Dipartimento della protezione civile, Roma, 61.

Loke, M. H. and R. D. Barker (1996a). Rapid least-squares inversion of apparent resistivity pseudosections using a quasi-Newton method, Geophys. Prospect. 44, 1, 131-152, doi:10.1111/j.1365-2478.1996.tb00142.x.

Loke, M. H. and R. D. Barker (1996b). Practical techniques for 3D resistivity surveys and data inversion, Geophys. Prospect., 44, 3, 499-523, doi:10.1111/j.1365-2478.1996.tb00162.x.

Loke, M. H., J. E. Chambers, D. F. Rucker, O. Kuras and P. B. Wilkinson (2013). Recent developments in the direct-current geoelectrical imaging method, J. Appl. Geophys., 95, 135-156, doi:10.1016/j.jappgeo.2013.02.017.

Nakamura, Y. (1989). A method for dynamic characteristics estimation of subsurface using microtremor on the ground surface. QR Railway Technical Research Institute 30, 25-33.

Nogoshi, M. and T. Igarashi (1970). On the propagation characteristics of microtremors, J. Seism. Soc. Japan 23: 264-280 (in Japanese with English abstract).

Park, C. B., R. D. Miller and J. Xia (1999) Multichannel analysis of surface waves. Geophysics 64: 800-808.

Park, C. B., R. D. Miller, J. Xia and J. Ivanov (2007). Multichannel analysis of surface waves (MASW) – active and passive methods. The Leading Edge, 26, 1, doi:10.1190/1.2431832.

Romagnoli, G., F. Pavano, G. Tortorici and S. Catalano (2021). Field dataset of the 2018 Mount Etna earthquake (Mw 4.9), Mendeley Data, doi:10.17632/rzmdnj8j2w.4.

Servizio Geologico D'Italia – SGI (2009). Carta Geologica d'Italia alla scala 1:50.000, F. 625 "Acireale". ISPRA, Roma.

SESAME (2004). Guidelines for the implementation of the H/V spectral ratio technique on ambient vibrations: Measurements, processing and interpretation. European Research Project SESAME (Deliverable D23.12), https://sesame.geopsy.org/Delivrables/Del-D23-HV_User_Guidelines.pdf.

Tortorici, G., F. Pavano, G. Romagnoli and S. Catalano (2021). The effect of recent resurfacing in volcanic areas on the distribution of co-seismic ground deformation due to strike-slip earthquakes: new insights from the 12/26/2018 seismic event at Mt. Etna, J. Struct. Geol., 145, doi:10.1016/j.jsg.2021.104308.

Tringali, G., D. Bella, F. A. Livio, M. F. Ferrario et al. (2021). Fault rupture and aseismic creep accompanying the December 26, 2018, Mw 4.9 Fleri earthquake (Mt. Etna, Italy): factors affecting the surface faulting in a volcano-tectonic environment, Quaternary Int., doi:10.1016/j.quaint.2021.124.019.

***CORRESPONDING AUTHOR: Grazia CAIELLI**,
Istituto di Geoscienze, Consiglio Nazionale delle Ricerche, Italy
e-mail: graziamaria.caielli@cnr.it

© 2026 the Author(s).
Open Access. This article is licensed under a Creative Commons Attribution 4.0 International License